Technical Report

The Use of Hydroacoustic Phases for the Detection of Oceanic Events: Observations and Numerical Modeling

Approved for public release; distribution is unlimited.

July 2004

Prepared for:
Defense Threat Reduction Agency
87/25 John J. Kingman Road, MS-6201
Fort Belvoir, VA 22060-6201

DSWA01-97-C-0162

Catherine de Groot-Hedlin, et. al

Prepared by:

University of California–San Diego
Scripps Institution of Oceanography
P.O. Box 6049
San Diego, CA 92166-6049

20040915 209

REPORT DOCUMENTATION PAGE

Form Approved

Public reporting burden for this collection of information is estimated to average 1 hour per response, including the time for reviewing instructions, searching existing data sources, gathering and maintaining the data needed, and completing and reviewing the collection of information. Send comments regarding this burden, estimate or any other aspect of this collection of information, including suggestions for reducing this burden, to Washington Headquarters Services, Directorate for Information Operations and Reports, 1215 Jefferson Davis Highway, Suite 1204, Arlington, VA 22202-4302, and to the Office of Management and Budget, Paperwork Reduction Project (0704-0188), Washington, DC 20503.

1. AGENCY USE ONLY (*Leave blank*)	2. REPORT DATE July 2004	3. REPORT TYPE AND DATES COVERED Technical 930929-990628

4. TITLE AND SUBTITLE The Use of Hydroacoustic Phases for the Detection of Oceanic Events: Observations and Numerical Modeling	5. FUNDING NUMBERS C – DSWA01-97-C-0162 PE – 4613 PR – CD TA – CD WU – DH 65183
6. AUTHOR(S) Catherine de Groot-Hedlin, Donna Blackman and John Orcutt	

7. PERFORMING ORGANIZATION NAME(S) AND ADDRESS(ES) University of California – San Diego Scripps Institution of Oceanography. P.O. Box 609 San Diego, CA 92166-6049	8. PERFORMING ORGANIZATION REPORT NUMBER

9. SPONSORING/MONITORING AGENCY NAME(S) AND ADDRESS(ES) Defense Threat Reduction Agency 8725 John J. Kingman Road, MS-6201 Fort Belvoir, VA 22060-6201 TDCN/Barber	10. SPONSORING/MONITORING AGENCY REPORT NUMBER DTRA-TR-01-33

11. SUPPLEMENTARY NOTES

This work was sponsored by the Defense Threat Reduction Agency under RDT&E RMC Code B 4613 D CD CD 65183 C340 A 25904D.

12a. DISTRIBUTION/AVAILABILITY STATEMENT Approved for public release; distribution is unlimited.	12b. DISTRIBUTION CODE

13. ABSTRACT (*Maximum 200 words*)

Hydroacoustic monitoring of the CTBT requires the ability to detect and locate phenomena that give rise to acoustic signals. An improved understanding of the coupling of seismic energy to acoustic energy to acoustic energy is necessary to improve location estimates of earthquakes and volcanic eruptions. Using known variations in near-source bathymetry, we demonstrated that scattering of seismic to acoustic energy at a rough seafloor yields the approximate time-frequency characteristics of T-phases excited both at shallow regions within the SOFAR channel, as well as at abyssal depths far below the sound channel. We also found that long-range acoustic propagation models predict wider and deeper shadow zones behind islands for high resolution bathymetric datasets that for the more coarsely gridded ETOPO5 data.

Furthermore, we exploited hydrophone and seismic waveform to analyze signals from natural events, such as underwater earthquakes. It is clear that offshore hydrophones, even in subpolar regions where the sound channel is not well defined, have lower recording thresholds for small to moderate oceanic events than do onshore seismic stations in the region surrounding an oceanic basin. For the Norwegian Sea study, we detected 2-3 orders of magnitude more events than were located by onshore seismic arrays.

14. SUBJECT TERMS Hydroacoustic Acoustic Modes Seismic to Accoustic Mohns Ridge		15. NUMBER OF PAGES 68
		16. PRICE CODE

17. SECURITY CLASSIFICATION OF REPORT UNCLASSIFIED	18. SECURITY CLASSIFICATION OF THIS PAGE UNCLASSIFIED	19. SECURITY CLASSIFICATION OF ABSTRACT UNCLASSIFIED	20. LIMITATION OF ABSTRACT SAR

NSN 7540-01-280-5500

Standard Form 298 (Rev. 2-89)
Prescribed by ANSI Sta. 239-1298-102

SUMMARY

Hydroacoustic monitoring of the CTBT requires the ability to detect and locate phenomena that give rise to acoustic signals. An improved understanding of the coupling of seismic energy to acoustic energy is necessary to improve location estimates of earthquakes and volcanic eruptions. Using known variations in near-source bathymetry, we demonstrated that scattering of seismic to acoustic energy at a rough seafloor yields the approximate time-frequency characteristics of T-phases excited both at shallow regions within the SOFAR channel, as well as at abyssal depths far below the sound channel. The modeling predicts that T-phases are generated most efficiently at shallow depths, and consist mainly of low order acoustic modes. Abyssal phases, which are excited at depths of several kilometres, consist of high order acoustic modes that interact weakly with the seafloor along much of the transmission path but can have significant amplitude for paths with few bathymetric obstacles.

An improved understanding of the accuracy needed for various input parameters to long-range acoustic propagation models, such as bathymetry and temperature data, is essential both in predicting acoustic shadow regions, and in estimating source locations. We found that long-range acoustic propagation models predict wider and deeper shadow zones behind islands for high resolution bathymetric datasets than for the more coarsely gridded ETOPO5 data. Seasonal variations in modal group velocity can reach up to 4mm/sec, which could translate to a time difference of 9 sec. over a 5000km path. This is only a small source of error compared to the large errors routinely made in picking T-phase arrivals from earthquakes.

Furthermore, we exploited hydrophone and seismic waveform to analyze signals from natural events, such as underwater earthquakes. It is clear that offshore hydrophones, even in subpolar regions where the sound channel is not well defined, have lower recording thresholds for small to moderate oceanic events than do onshore seismic stations in the region surrounding an oceanic basin. For the Norwegian Sea study, we detected 2-3 orders of magnitude more events than were located by onshore seismic arrays.

CONVERSION TABLE

Conversion Factors for U.S. Customary to metric (SI) units of measurement.

MULTIPLY ⟶ BY ⟶ TO GET

TO GET ⟵ BY ⟵ DIVIDE

angstrom	1.000 000 x E -10	meters (m)
atmosphere (normal)	1.013 25 x E +2	kilo pascal (kPa)
bar	1.000 000 x E +2	kilo pascal (kPa)
barn	1.000 000 x E -28	meter^2 (m^2)
British thermal unit (thermochemical)	1.054 350 x E +3	joule (J)
calorie (thermochemical)	4.184 000	joule (J)
cal (thermochemical/cm^2)	4.184 000 x E -2	mega joule/m^2 (MJ/m^2)
curie	3.700 000 x E +1	*giga bacquerel (GBq)
degree (angle)	1.745 329 x E -2	radian (rad)
degree Fahrenheit	$t_k = (t°f + 459.67)/1.8$	degree kelvin (K)
electron volt	1.602 19 x E -19	joule (J)
erg	1.000 000 x E -7	joule (J)
erg/second	1.000 000 x E -7	watt (W)
foot	3.048 000 x E -1	meter (m)
foot-pound-force	1.355 818	joule (J)
gallon (U.S. liquid)	3.785 412 x E -3	meter^3 (m^3)
inch	2.540 000 x E -2	meter (m)
jerk	1.000 000 x E +9	joule (J)
joule/kilogram (J/kg) radiation dose absorbed	1.000 000	Gray (Gy)
kilotons	4.183	terajoules
kip (1000 lbf)	4.448 222 x E +3	newton (N)
kip/inch^2 (ksi)	6.894 757 x E +3	kilo pascal (kPa)
ktap	1.000 000 x E +2	newton-second/m^2 (N-s/m^2)
micron	1.000 000 x E -6	meter (m)
mil	2.540 000 x E -5	meter (m)
mile (international)	1.609 344 x E +3	meter (m)
ounce	2.834 952 x E -2	kilogram (kg)
pound-force (lbs avoirdupois)	4.448 222	newton (N)
pound-force inch	1.129 848 x E -1	newton-meter (N-m)
pound-force/inch	1.751 268 x E +2	newton/meter (N/m)
pound-force/foot^2	4.788 026 x E -2	kilo pascal (kPa)
pound-force/inch^2 (psi)	6.894 757	kilo pascal (kPa)
pound-mass (lbm avoirdupois)	4.535 924 x E -1	kilogram (kg)
pound-mass-foot^2 (moment of inertia)	4.214 011 x E -2	kilogram-meter^2 (kg-m^2)
pound-mass/foot^3	1.601 846 x E +1	kilogram-meter^3 (kg/m^3)
rad (radiation dose absorbed)	1.000 000 x E -2	**Gray (Gy)
roentgen	2.579 760 x E -4	coulomb/kilogram (C/kg)
shake	1.000 000 x E -8	second (s)
slug	1.459 390 x E +1	kilogram (kg)
torr (mm Hg, 0° C)	1.333 22 x E -1	kilo pascal (kPa)

*The bacquerel (Bq) is the SI unit of radioactivity; 1 Bq = 1 event/s.
**The Gray (GY) is the SI unit of absorbed radiation.

TABLE OF CONTENTS

TABLE OF CONTENTS (CONTINUED)

Table of Figures

Section 1
Introduction

1.1 Research Objectives.

Hydroacoustic monitoring of the Comprehensive Nuclear Test Ban Treaty (CTBT) requires the ability to detect and locate phenomena that give rise to acoustic signals, and to distinguish explosions from naturally occuring events, such as suboceanic explosions and volcanoes. An improved understanding of the accuracy needed for various input parameters to long-range acoustic propagation models, such as bathymetry and temperature data, is essential both in predicting acoustic shadow regions, and in estimating source locations. We performed numerical computations of acoustic propagation using both fine-scale and relatively coarse bathymetric datasets, to analyze the the accuracy needed in predicting acoustic transmission. The effect of seasonal variations in temperature on acoustic travel times is also examined. Furthermore, an improved understanding of the coupling of seismic energy to acoustic energy is necessary to improve location estimates of earthquakes and volcanic eruptions along active ridges and convergence zones. We modeled the transition from seismic to acoustic propagation using known variations in near-source geology and bathymetry. Finally, we exploit hydrophone and seismic waveform data available through the International Data Center (IDC) as well as SOSUS waveform data, to analyze signals from natural events, such as underwater earthquakes. Emphasis is placed both on events in the North Atlantic and North Pacific oceans.

1.2 Background.

1.2.1 The Acoustic Waveguide.
One of the challenges of modeling acoustic transmissions on a global scale is to obtain accurate input data to describe adequately the complexity of the waveguide. The quantity of information necessary is related to the wavelength modeled; densely-sampled databases which contain good quality information on both sound-speed profiles and bottom depth are necessary to model acoustic transmissions up to high frequencies. This information is necessary both to determine the propagation path and to compute transmission loss along that path. Computation of the travel path is a 3-D problem given that lateral variations in temperature and bathymetry affect phase speeds. Because sound energy is refracted away from regions of higher phase velocity, acoustic energy bends away from regions of shallow depth, such as islands and seamounts (Munk and Zachariasen, 1991). Adiabatic Mode Parabolic Equation (AMPE) modeling (Collins, 1993), has been shown to be a practical technique for computing global-scale acoustic transmission at low frequencies (Collins et.al., 1995).

1.2.2 Seismic to Acoustic Energy Transition at the Seafloor.
Seismic events below the seafloor generate ocean-borne acoustic phases, called T-phases, that propagate great distances within the ocean sound channel minimum with little transmission loss. Early hydroacoustic recordings indicated that T-phases are excited in shallow regions where the seafloor is sloping, *i.e.* near islands or submarine promontories, and not necessarily at the earth-

1

quake epicenters (Shurbet and Ewing, 1957; Johnson and Norris,1963). This "slope" T-phase often features multiple peaks associated with bathymetric highs in the vicinity of the epicenter (Shurbet and Ewing, 1957; Johnson and Norris,1963; Walker *et.al,* 1992), thus the source region can often be recognized by its signal characteristics (Johnson *et.al.,* 1963). Another class of seismically-generated acoustic phases, with source locations coincident with earthquake epicenters far below the ocean sound channel, was later identified (Johnson and Norris,1963; Johnson *et.al.,* 1968). These "abyssal" T-phases are characterized by a higher dominant frequency than that of the slope T-phase, and by symmetric coda about the peak frequency arrivals (Keenan and Merriam, 1991). Abyssal T-phases are often weaker than those generated in shallow regions, further from the epicenter (Johnson *et.al.,* 1963).

The distinct characteristics of the slope and abyssal T-phases are widely thought to derive from distinct seismic to acoustic coupling mechanisms (*e.g.* Johnson and Norris,1963; Johnson *et.al.,* 1968; Keenan and Merriam, 1991). Excitation of T-phases in shallow regions near islands or near the continental shelf is usually attributed to downslope propagation (Milne, 1959; Talandier and Okal, 1998), which occurs where steep slopes intersect the sound channel. In this description, acoustic energy is refracted nearly vertically into the ocean column and is transformed to a horizontally propagating phase by multiple reflections between the sea surface and sloping seafloor. However, de Groot-Hedlin and Orcutt (1999) showed that, for a gently sloping, sediment covered seafloor, the shape of the T-phase envelope is consistent with a coupling mechanism that is dependent mainly on depth rather than slope, and attributed the excitation of the slope T-phase to seafloor scattering. Excitation of the abyssal T-phase has variously been attributed to coupling between Stoneley waves and the SOFAR sound channel (Biot, 1952), and reflection scattering from either the seafloor or sea surface (Johnson *et.al.,* 1968) or from the overlying sea ice (Keenan and Merriam, 1991).

1.2.3 Seismo-Acoustic Detection in the Norwegian Sea.
The goals of our work in the Norwegian Sea were to evaluate the use of U.S. Navy North Atlantic hydrophone arrays in determining seismicity patterns and to assess how T-wave data could contribute to offshore event location and characterization as part of monitoring efforts for a nuclear test-ban treaty. In order to compare the offshore hydroacoustic capability with more standard onshore seismic resources, data from several onshore arrays in Norway were included in the study. A recording/archive facility for the hydrophone data was in operation from early 1995 until late 1996 so this is the time period covered by this aspect of our study.

1.3 Outline of Report.

This report is organized into 5 sections. In section 2, we analyze the dependence of modal group velocities on seasonal temperature variations, and compare numerical computations of acoustic blockage using several bathymetric datasets. In section 3, we describe a physical mechanism for the coupling of seismic energy to ocean-borne acoustic phases. We show that the observed spectral characteristics of seismically generated acoustic phases are consistent with excitation by Rayleigh scattering from a rough seafloor. In section 4, we examine a series of earthquakes recorded from November 1995 to January 1996 by onshore seismic stations and by U.S. Navy hydrophone arrays in the North Atlantic. We describe the refinement of epicenters using P, S (converted to an acoustic phase at the seafloor), and T-waves in the hydrophone data. Section 5 contains the primary conclusions of this study.

Section 2
Development Of An Accurate Ocean Model

2.1 Seasonal Variations in T-phase Velocity.

Acoustic velocities are computed using a nine term formula (Mackenzie,1981) relating salinity, temperature, and depth to sound velocity. Temperatures and salinity profiles are derived from the WOA database (Levitus and Boyer, 1994). Surface temperatures, and to a lesser extent, salinities, vary over the year thus the acoustic velocity model is a function of time. In Figure 1, we examine acoustic velocity profiles and group velocities for each month at 50N, 180E. As shown in the top left panel both the SOFAR channel velocity and depth vary over the year. Below approximately 500m, velocities are constant. Mode shapes, shown in Figure 1, are nearly constant over the year. Ocean-borne sound energy propagates at the modal group velocities (Heaney *et.al.,* 1991), plotted for the first few modes for f=5Hz, left, and f=10Hz, right. Velocity variations over the year are only on the order of nearly 4mm/sec, which translates to a time difference of 9 sec over a 5000km path. Although this translates to an event mislocation of approximately 13km, this is only a small source of error compared to the large errors routinely made in picking T-phase arrivals from earthquakes. Note that these computations were done for a deep water profile at a nearly polar latitude. Velocity variations at equatorial latitudes are less severe, due to less severe variations in surface temperature. On the other hand, seasonal velocity variations in shallow water are slightly greater, since the modal propagation is confined to the upper, more variable part of the ocean column.

2.2 Resolution of Bathymetric Datasets.

Bathymetry from the ETOPO5 database, which has a resolution of 5 minutes in both latitude and longitude, has often been used to constrain ocean bottom depths for global-scale acoustic transmission. This sampling is rather coarse even for calculation of low frequency frequency transmissions, i.e. 1 Hz (Collins, 1995). A bathymetric dataset by Smith and Sandwell (1997) was computed by using shipboard depth surveys to calibrate the transfer function from satellite altimetry data to seafloor topography, and has become the new standard bathymetric dataset. This dataset resolves tectonic details to an accuracy usually within 100m in depth on a two minute grid. Where the seafloor is rugged, the error in depth is greater, as the method underestimates peak amplitudes at very tall seamounts. Accuracy also depends on the density of shipboard sounding data. Accuracy is substantially better in regions where more shipboard soundings are available, such as in both the North Pacific and North Atlantic.

In this section, we compare results of 3-D transmission loss computions at 5 Hz made using each of these datasets as the bathymetric input. 3-D transmission losses were computed using the adiabatic mode parabolic equation (AMPE) modeling code (Collins,1993), for hydrophones in the Atlantic and Pacific oceans. The AMPE method assumes that energy coupling between modes is negligible. The solutions provided by AMPE satisfy reciprocity, *i.e.* the source and receiver locations are interchangable within this formulation. The results of transmission loss computations for the first mode, for a sourceat the site of the ASC24 hydrophone is shown in Figure 2. In this case receiver depths (or equivalently, source depths for a receiver at ASC24) are all at 900m depth, the depth of the SOFAR channel near Ascension Island. Only one sound speed profile, accurate near Ascension
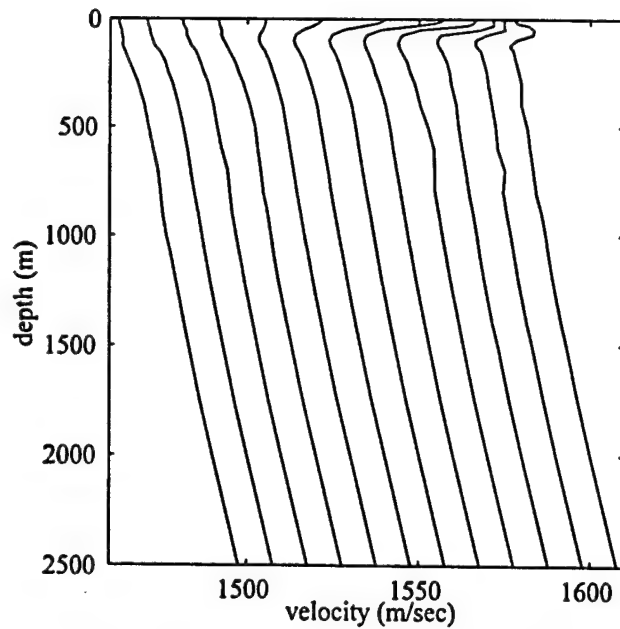
a) month by month velocity profiles at 50°N, 180°E, offset by 10m/sec.
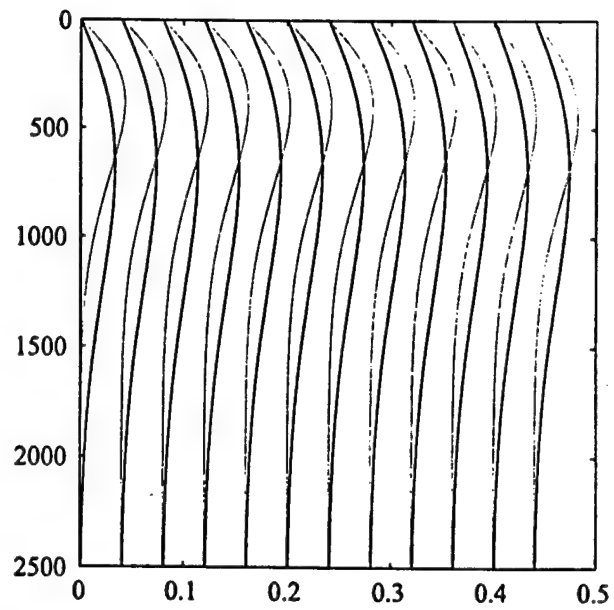
b) corresponding shape functions for mode 1 at f=5 Hz (dark line) and f=10Hz (light line).
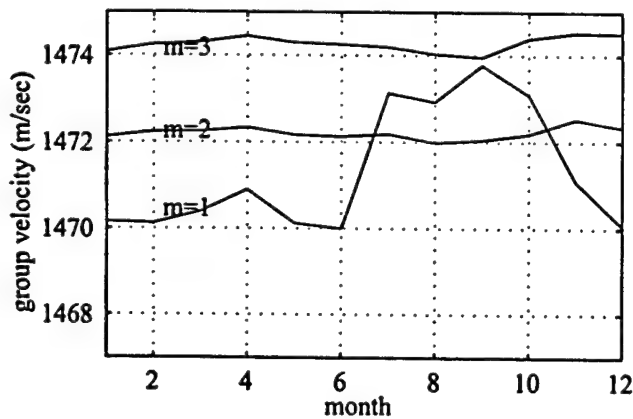
c) month by month variations in group velocities at f=5Hz for the first 3 modes.
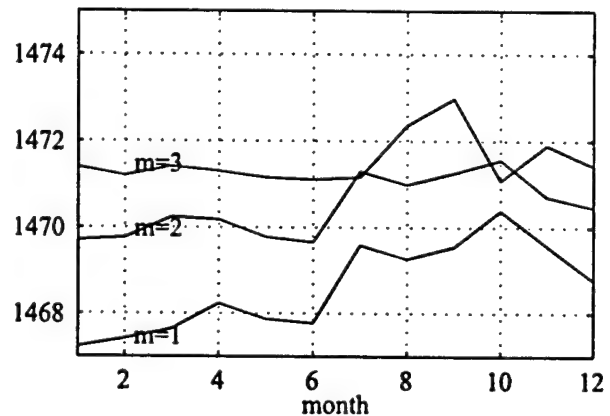
d) month by month variations in group velocity for f=10Hz, for the first 3 modes.

Figure 1. Variations in mode and group velocity over the year.
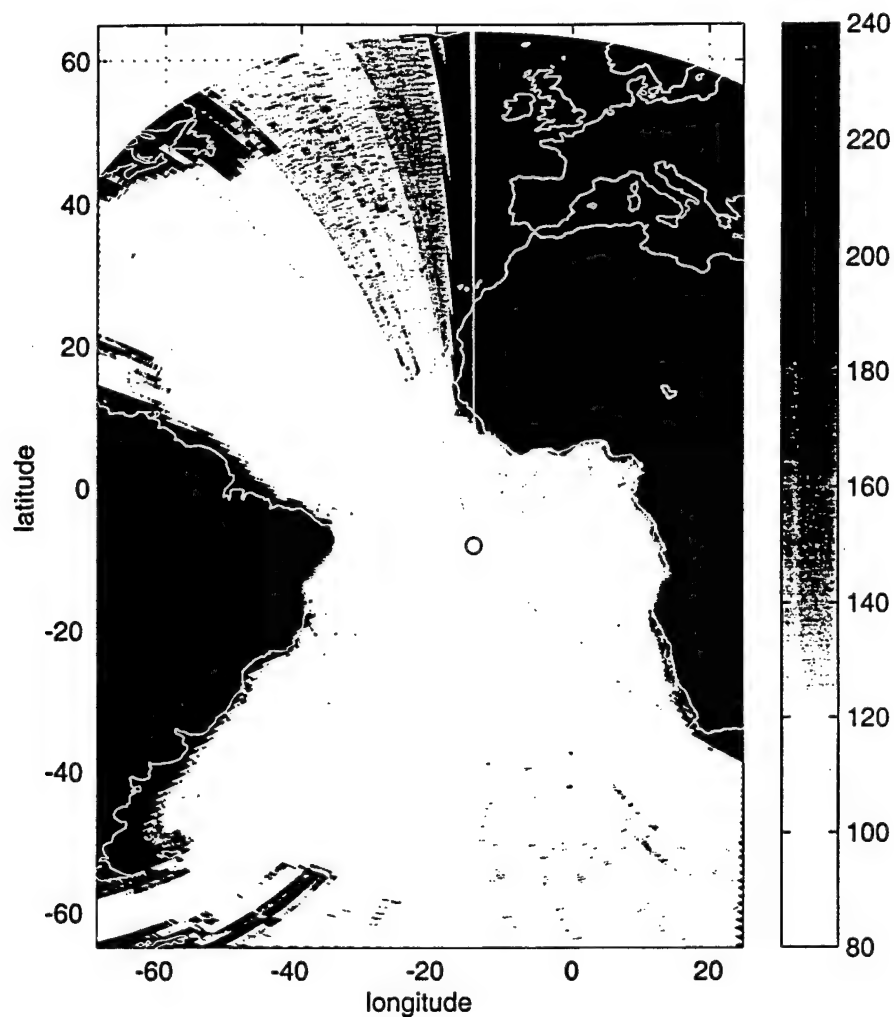
a) 2 minute bathymetry grid

Figure 2. Results of the AMPE computation of transmission loss for mode 1 at 5 Hz for a source located at ASC24. The source depth at ASC24 is 780m, the receiver depths are at 900m depth, i.e. at the sound channel minimum. By reciprocity, this plot gives the transmission loss for mode 1 at ASC24 for sources throughout the Atlantic at 900m depth.
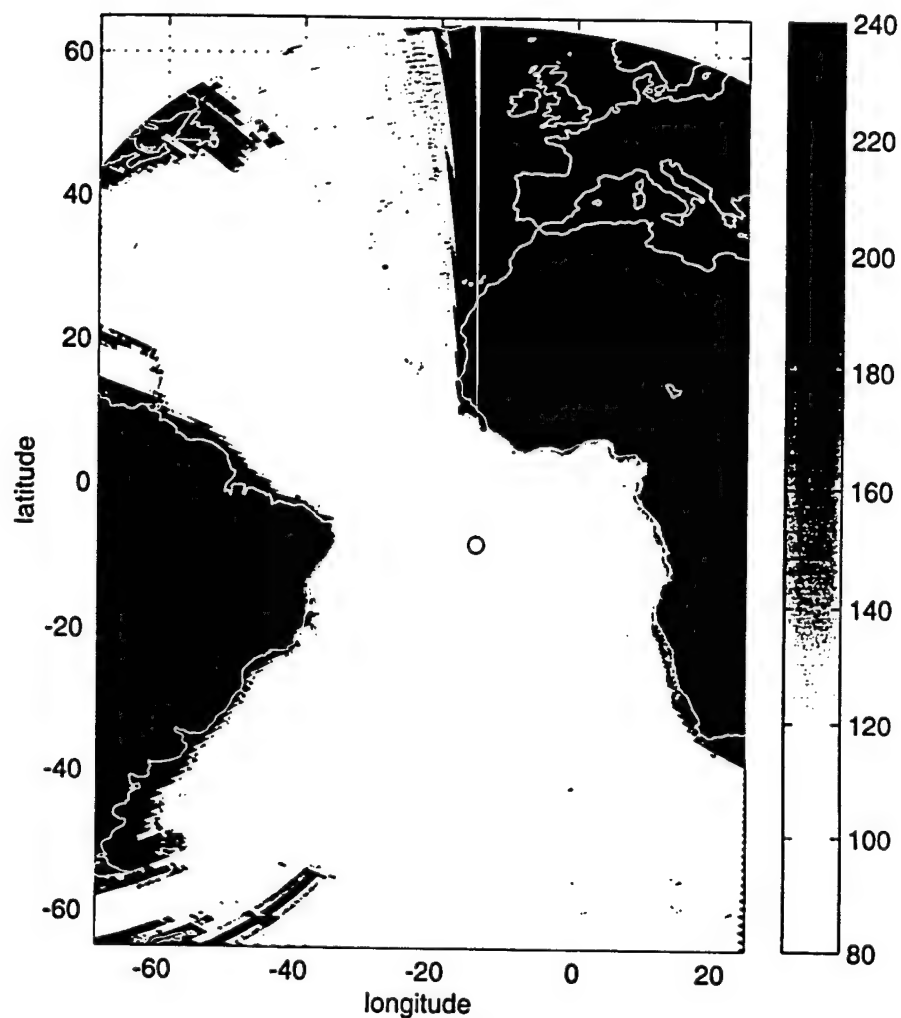
b) 5 minute bathymetry grid

Figure 2. Results of the AMPE computation of transmission loss for mode 1 at 5 Hz for a source located at ASC24. The source depth at ASC24 is 780m, the receiver depths are at 900m depth, i.e. at the sound channel minimum. By reciprocity, this plot gives the transmission loss for mode 1 at ASC24 for sources throughout the Atlantic at 900m depth.
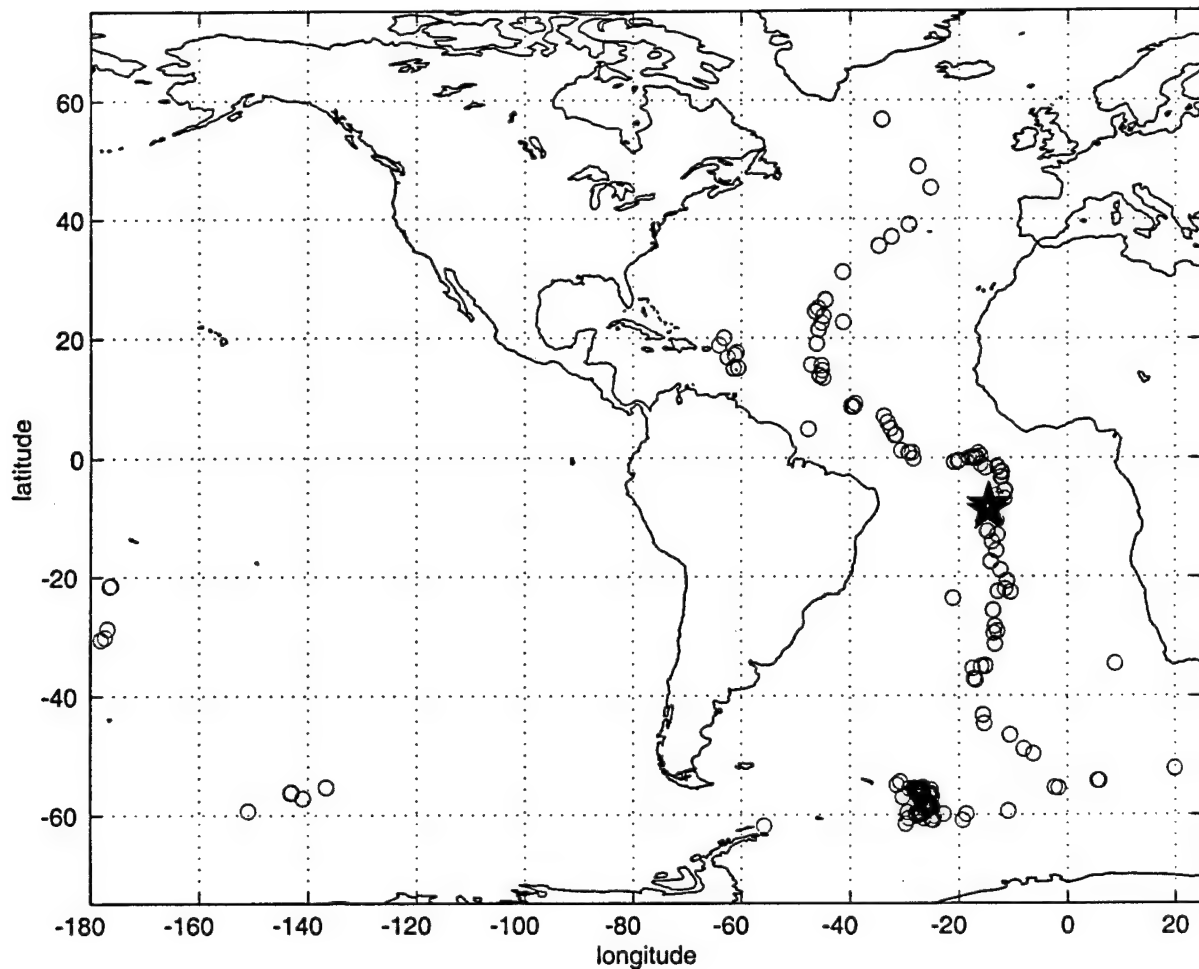
Figure 3. Circles mark epicentral locations of earthquakes in the Reviewed Event Bulletin (REB) for 1998-1999, published by the International Data Center (IDC), with associated T-phases identified at any of the hydrophones near Ascension Island. The dark stars indicate the location of the hydrophones at Ascension Island.

Island, is used for the entire Atlantic basin. Note that Smith and Sandwell (1997) bathymetry data yield a far wider shadow zone within the North Atlantic.

As a reality check, we mapped earthquake epicenters that were listed as having associated T-phases at any of the Ascension Island hydrophones by the IDC (Figure 3). Note that events that lie within the shadow zone for mode 1 are included here, probably because T-phases observed at any of the Ascension Island hydrophones are included for that figure. Note that T-phases were observed for a number of events in the Pacific Ocean.

Similar computations were performed for hydrophones at Pt Sur (Figure 2.4); events with associated T-phases are shown in Figure 5. In this case, the shadow zone to the east of the Aleutian island chain is correctly predicted by AMPE computations with either the ETOPO5 or Smith and Sandwell data.

7
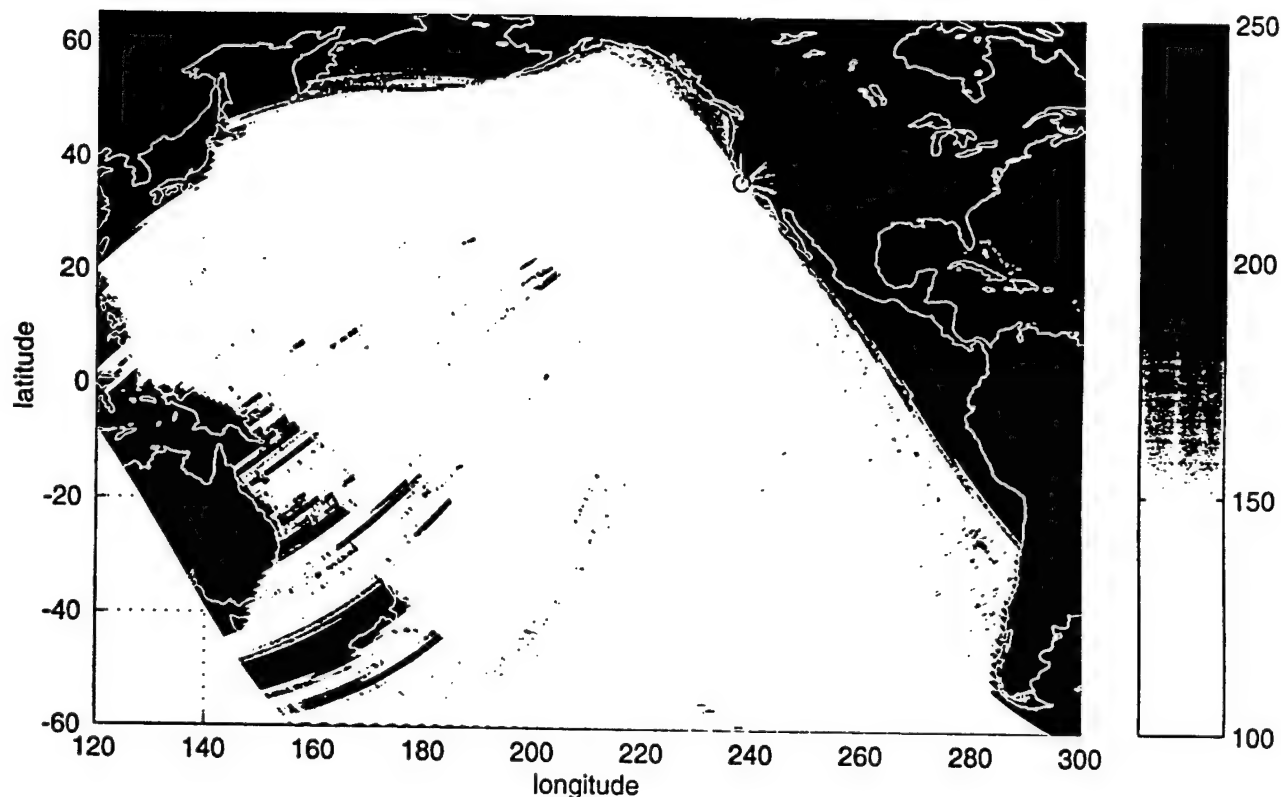
a) 2' grid (Smith and Sandwell, 1997)

Figure 4. Transmission loss for mode 1 at PSUR. The source depth at PSUR is 1425m, receiver depths are at 600m depth, *i.e.* at the sound channel minimum.

Overall, epicenters lying within predicted shadow zones do not have associated T-phases observable at Pt Sur. Figures 6 and 7 show similar results for WK30. (The thin dark wedge to the north northwest of WK30 is an artifact). Overall, the Smith and Sandwell data yield wider and deeper shadow zones behind islands than the ETOPO5 data.

Finally, 3-D transmission losses computed using both the Smith and Sandwell bathymetry and a much higher resolution bathymetric data set (Figure 8) were compared. Figure 9 shows results for AMPE computations at f=5Hz for a local region around Ascension Island. As shown, there are significant differences between the two solutions. To break down where these differences were arrising, separate computations were performed over the first four modes. Results are shown in Figure 10. As shown, the differences in transmission loss computed from each dataset increase with increasing mode number. This is to be expected since bottom interaction increases with increasing mode number, thus greater accuracy in the bathymetric database is required for higher mode numbers.

8
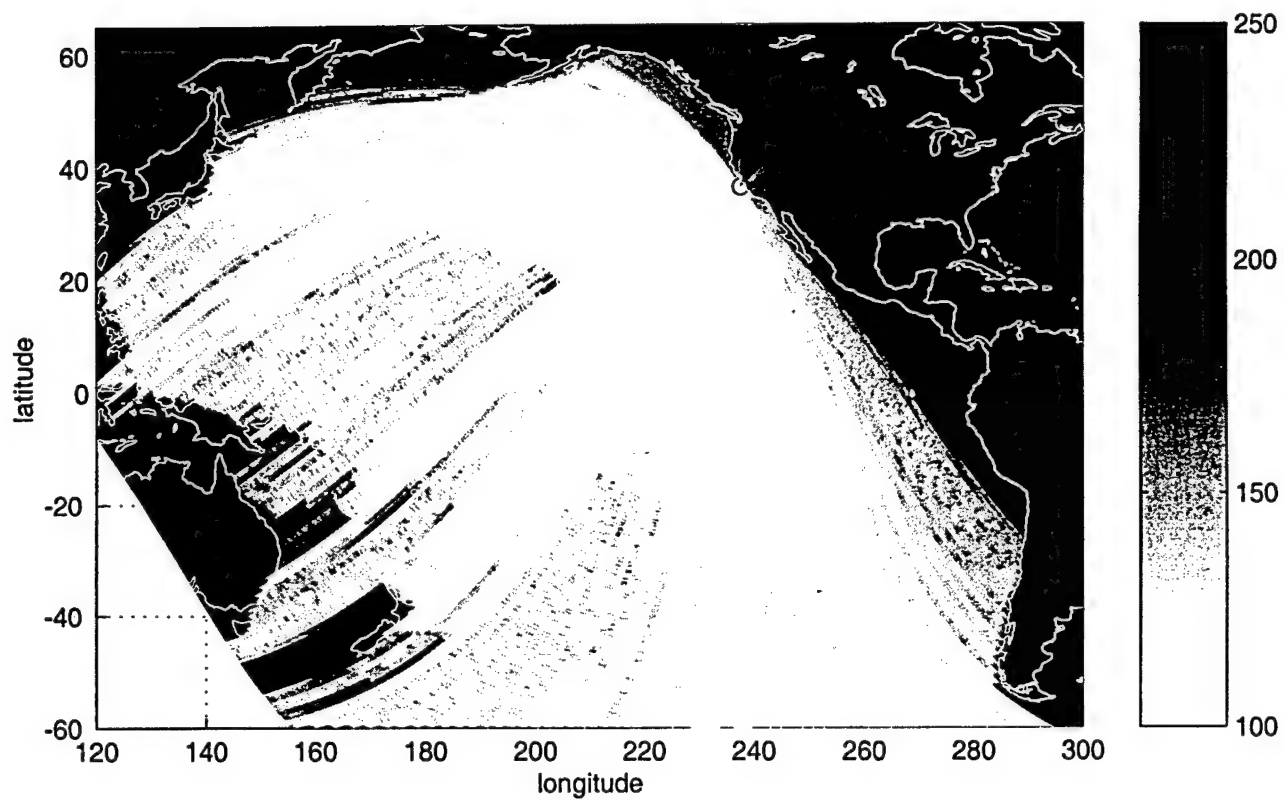
b) 5' grid using ETOPO5 bathymetry data

Figure 4. Transmission loss for mode 1 at PSUR. The source depth at PSUR is 1425m, receiver depths are at 600m depth, *i.e.* at the sound channel minimum.
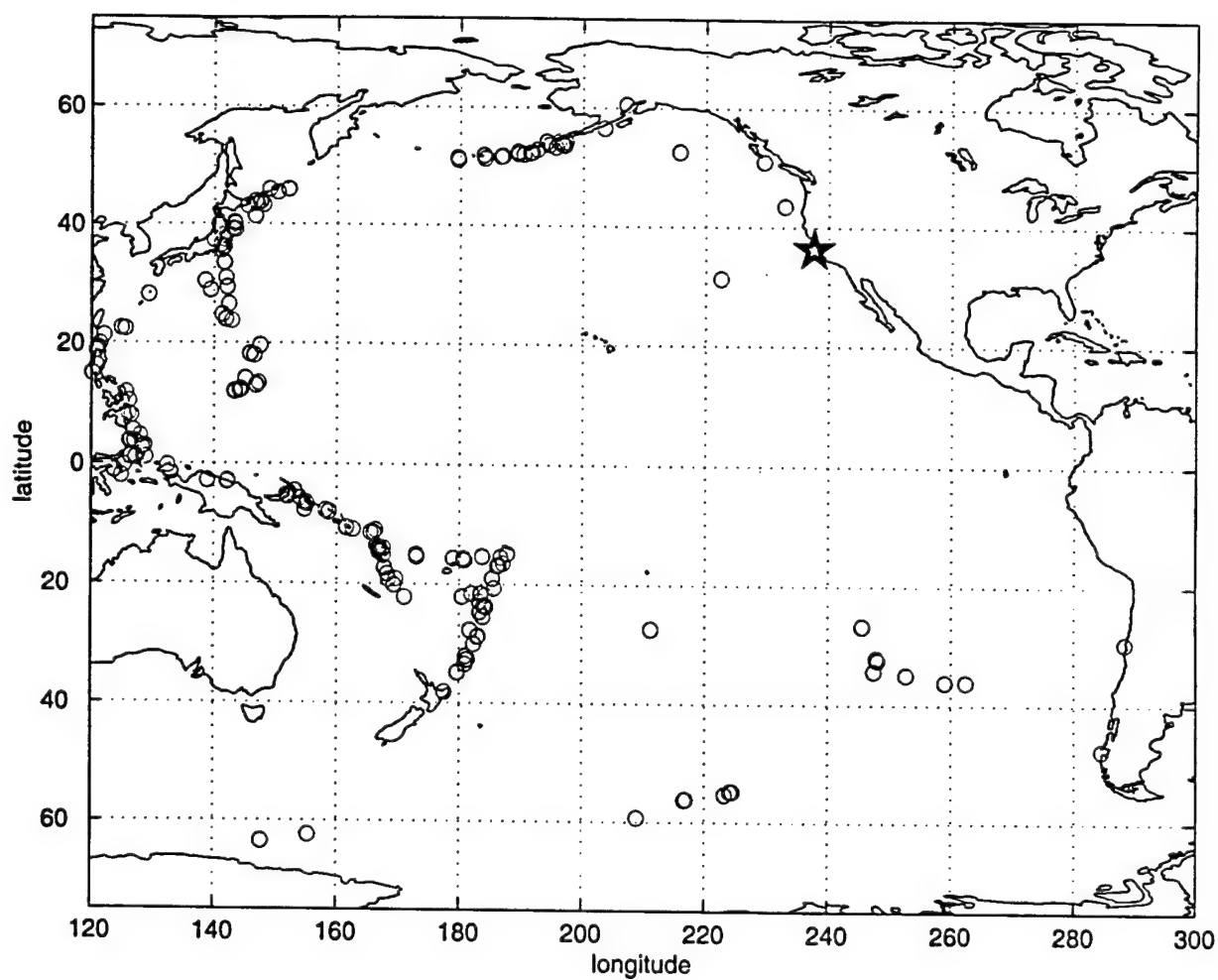
Figure 5. Circles mark the epicentral location of earthquakes published in the REB for 1998-1999, with associated T-phases identified at the Pt. Sur hydrophone. The dark star denotes the location of the Pt Sur hydrophone.

10
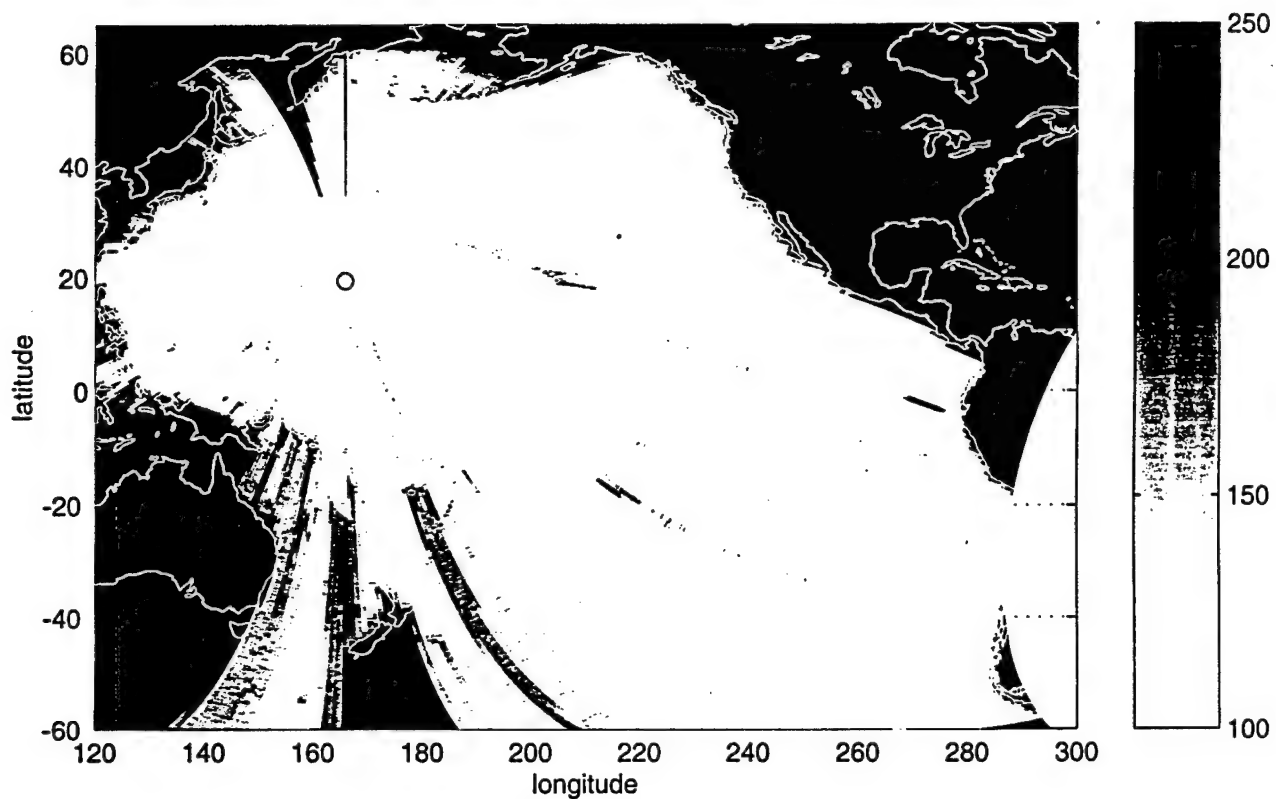
a) 2' grid (Smith and Sandwell, 1997)

Figure 6. Transmission loss for mode 1 at WK30, using Smith and Sandwell (1997) bathymetries. The source depth at WK30 is 812m, receiver depths are at 900m depth, *i.e.* at the sound channel minimum.
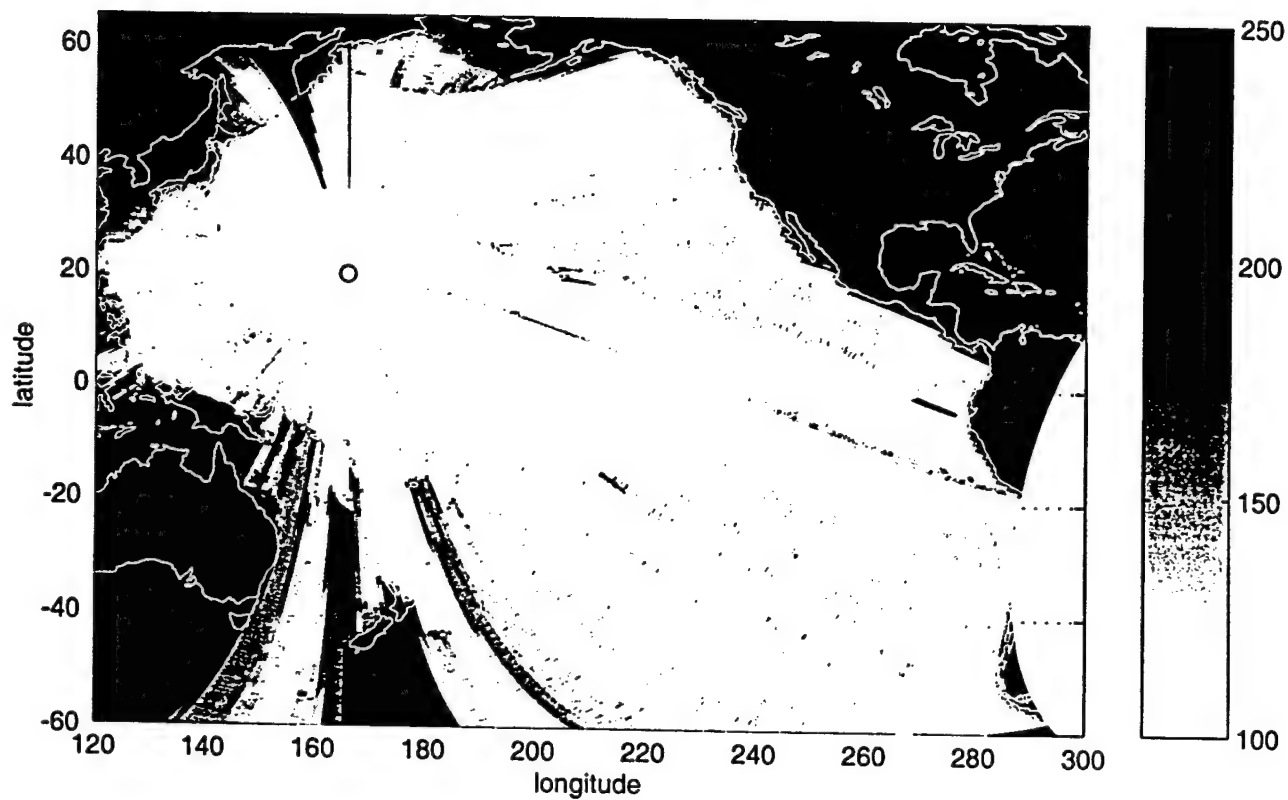
b) 5' grid using ETOPO% bathymetry data

Figure 6. Transmission loss for mode 1 at WK30.. The source depth at WK30 is 812m, receiver depths are at 900m depth, *i.e.* at the sound channel minimum.
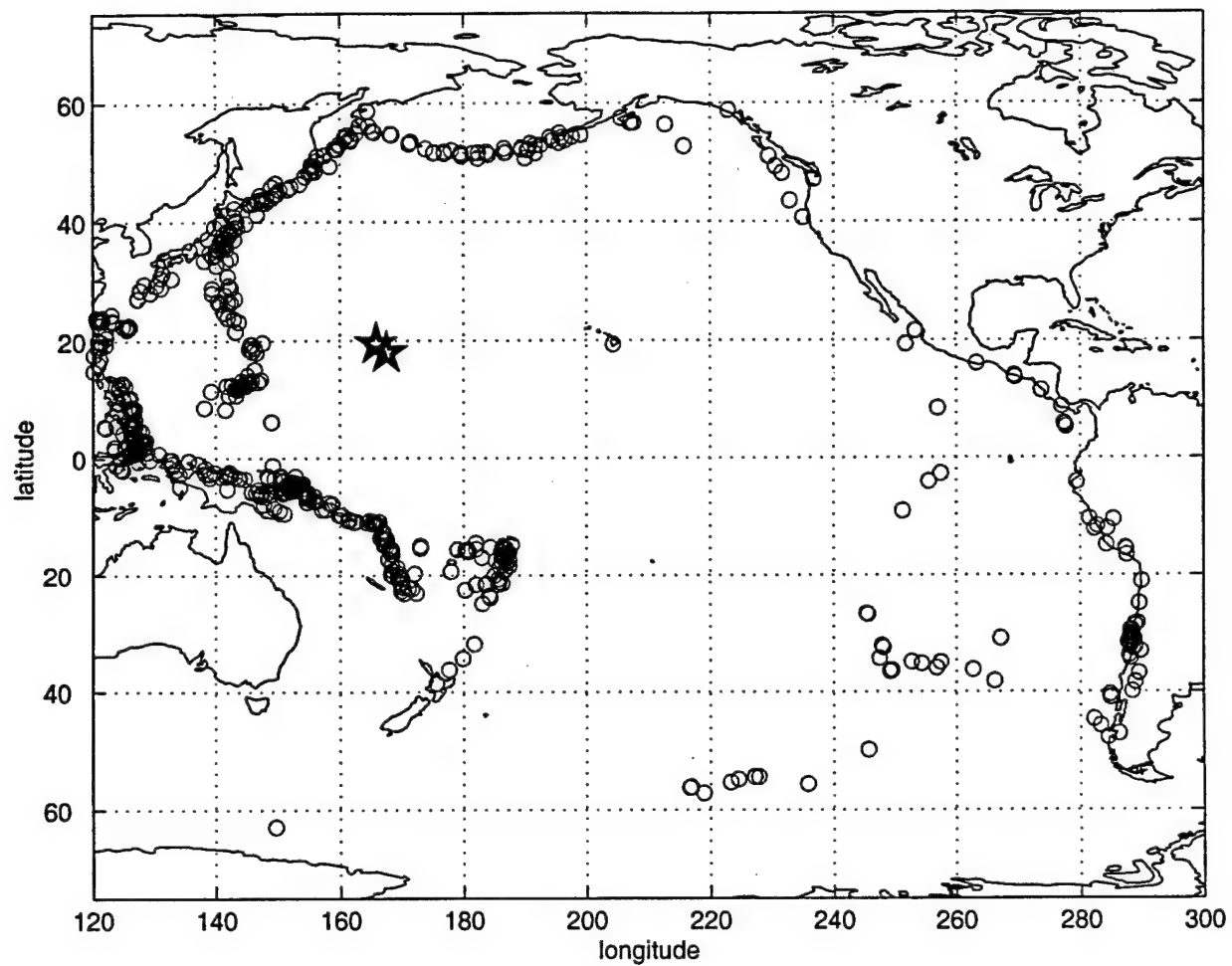
Figure 7. Circles mark the epicentral location of earthquakes published in the REB for 1998-1999, with associated T-phases identified at either of the Wake hydrophones. The dark stars denotes the location of the Wake hydrophones.
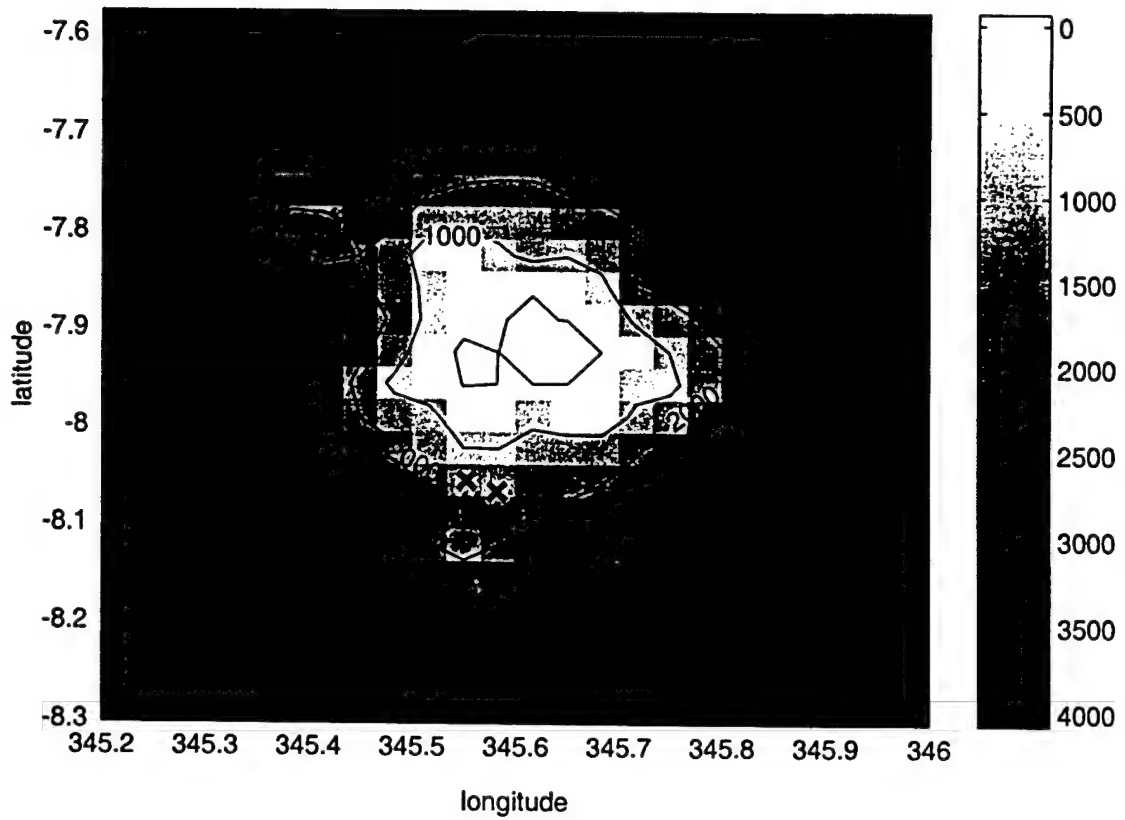
a) 2 minute bathymetry grid (Smith and Sandwell, 1997).

Figure 8   Comparison of bathymetry data. Hydrophones near Ascension are marked by X'es.
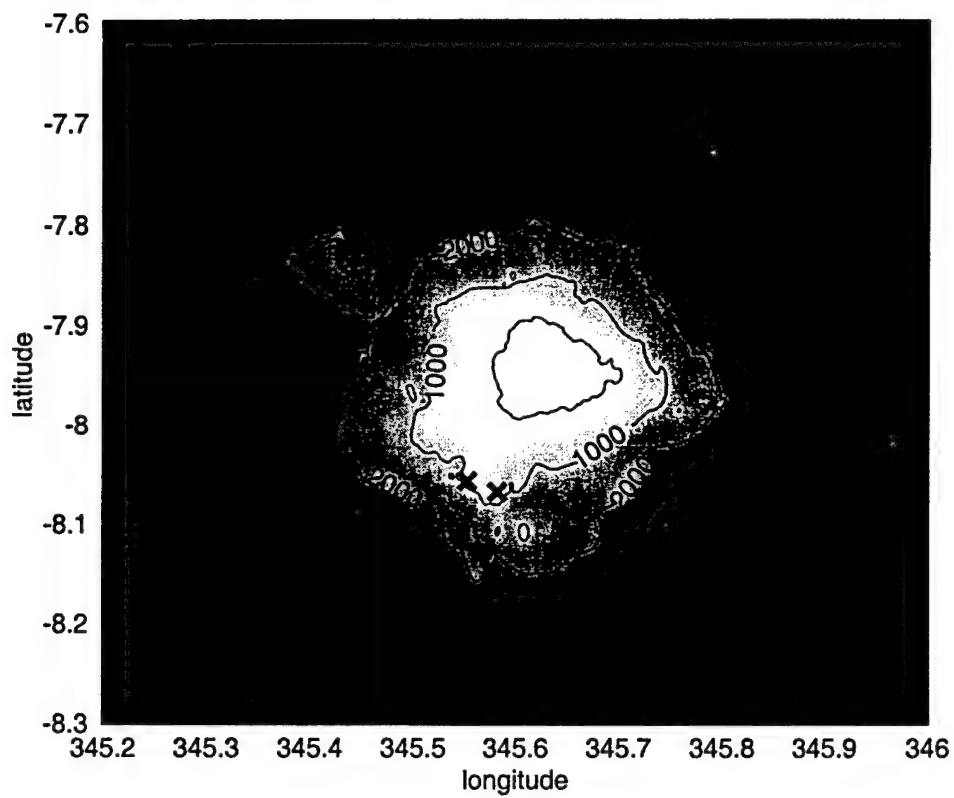
b) fine-scale bathymetry with gridpoints every 12" in latitude and 6" in longitude.

Figure 8   Comparison of bathymetry data. Hydrophones near Ascension are marked by X'es.
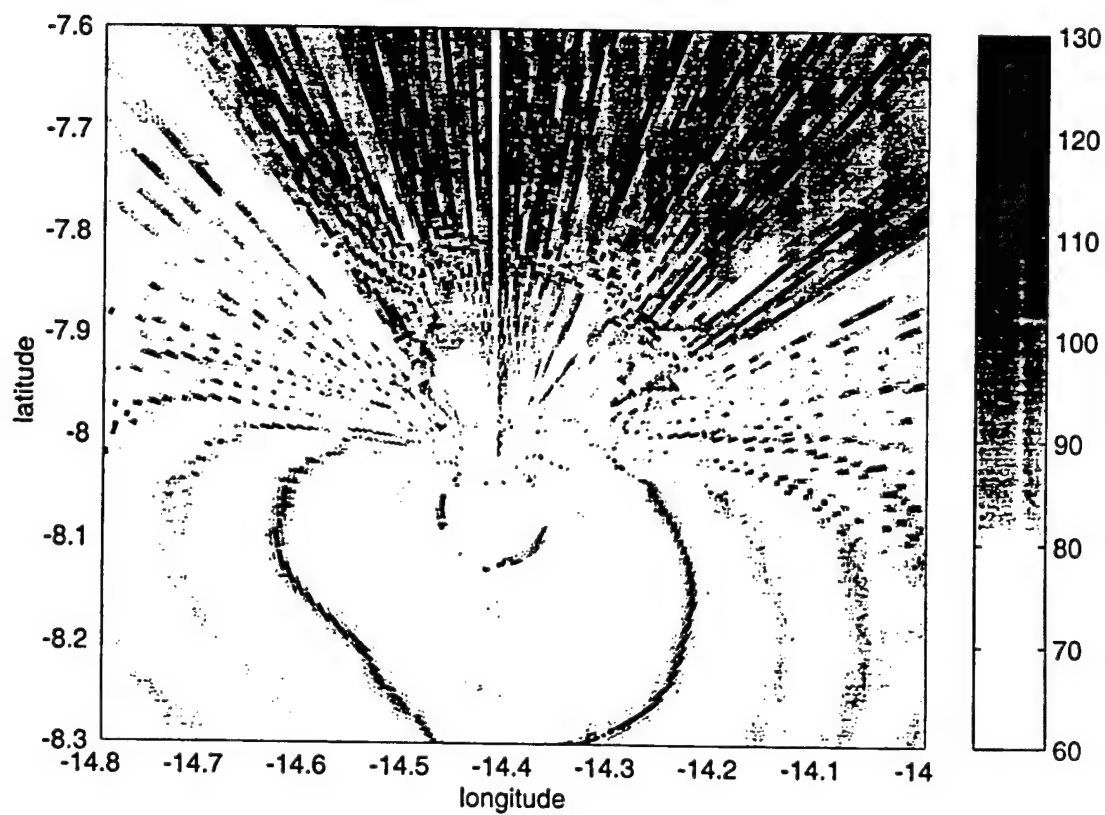
a) coarse bathymetry input.

Figure 9 Comparison of computed transmission losses at ASC24 for the first 5 modes.
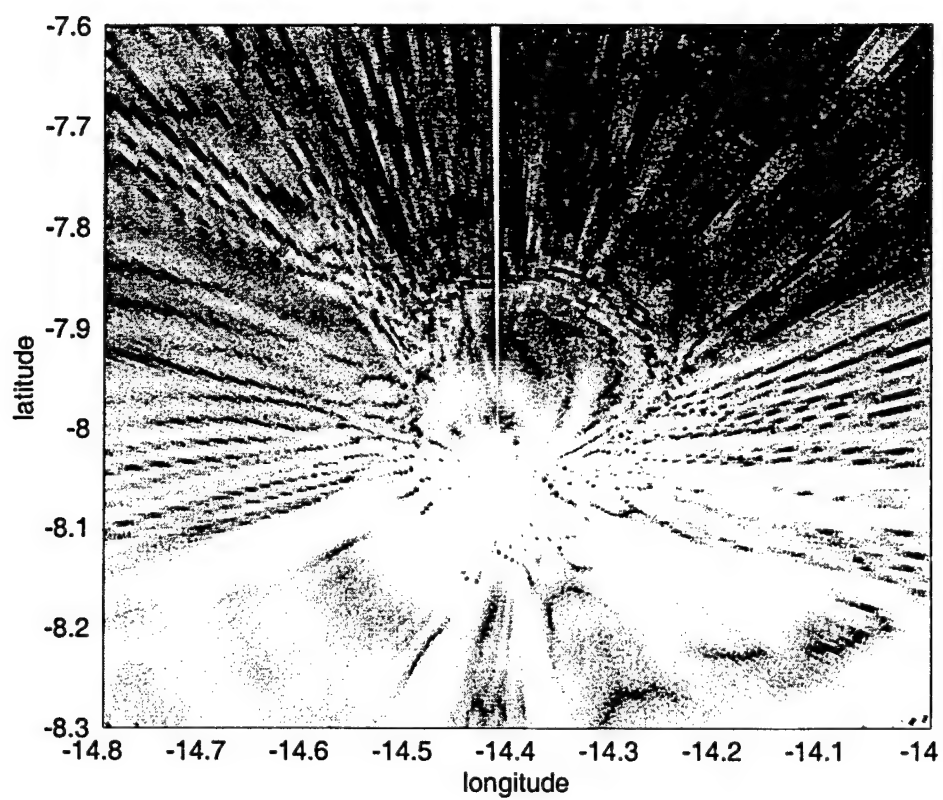
b) fine-scale bathymetry input.

Figure 9 Comparison of computed transmission losses at ASC24 for the first 5 modes.
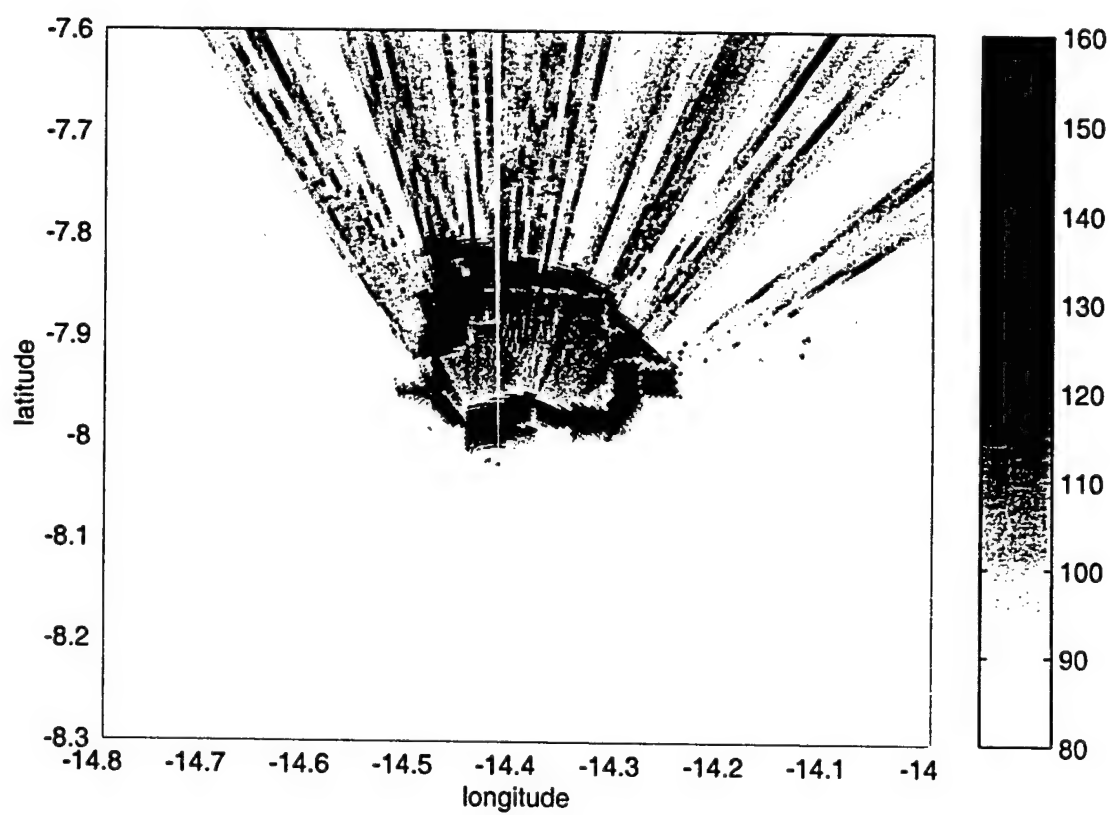
a) coarse bathymetry input.

Figure 10. Comparison of transmission loss computations at ASC24 for mode 1.
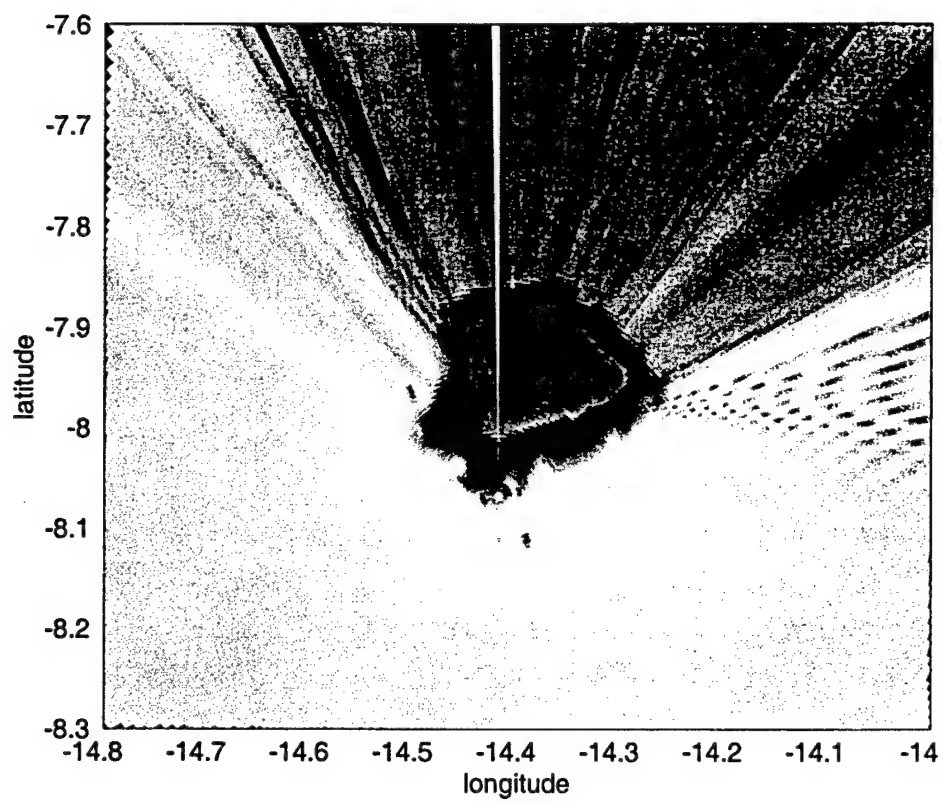
b) fine-scale bathymetry input.

Figure 10. Comparison of transmission loss computations at ASC24 for mode 1.
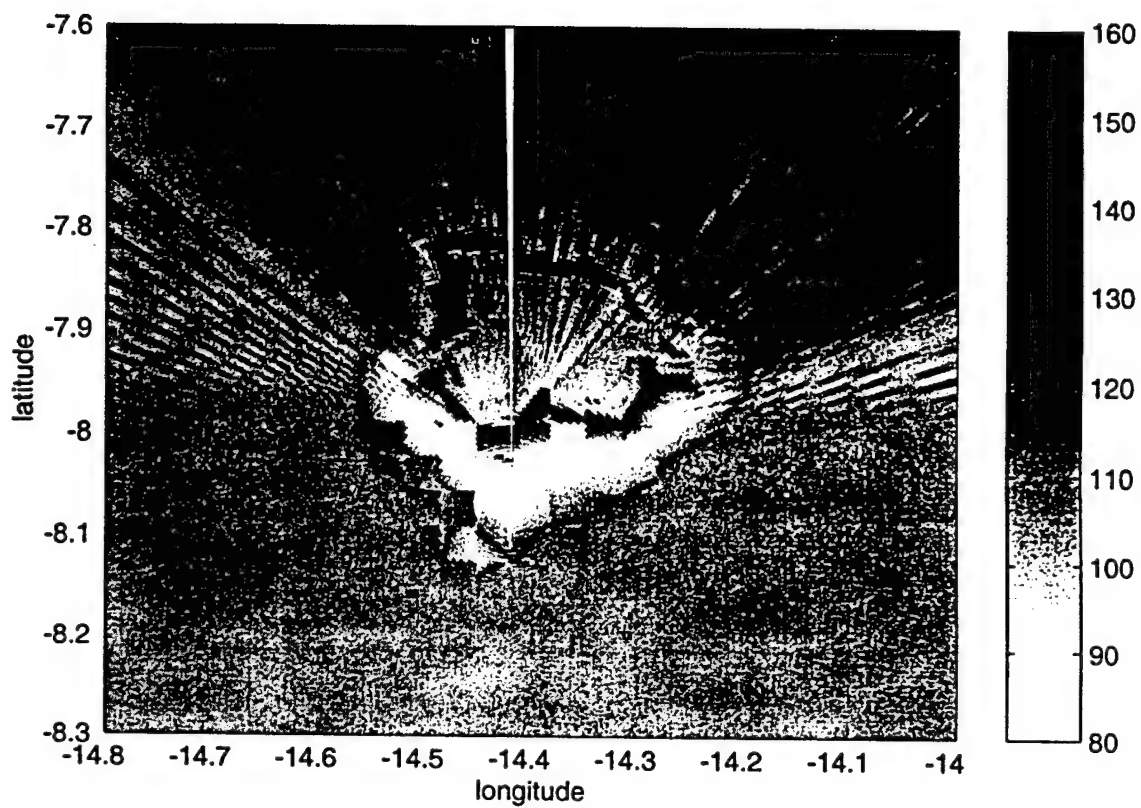
a) coarse bathymetry input.

Figure 11. Comparison of transmission loss computations at ASC24 for mode 2.
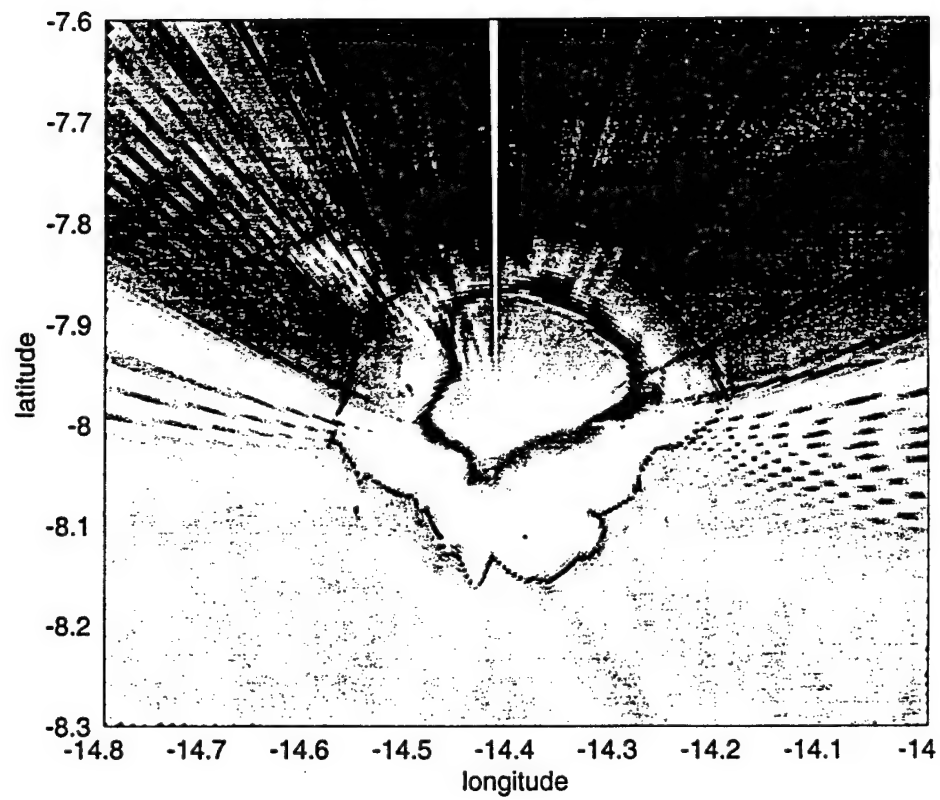
b) fine-scale bathymetry input.

Figure 11. Comparison of transmission loss computations at ASC24 for mode 2.
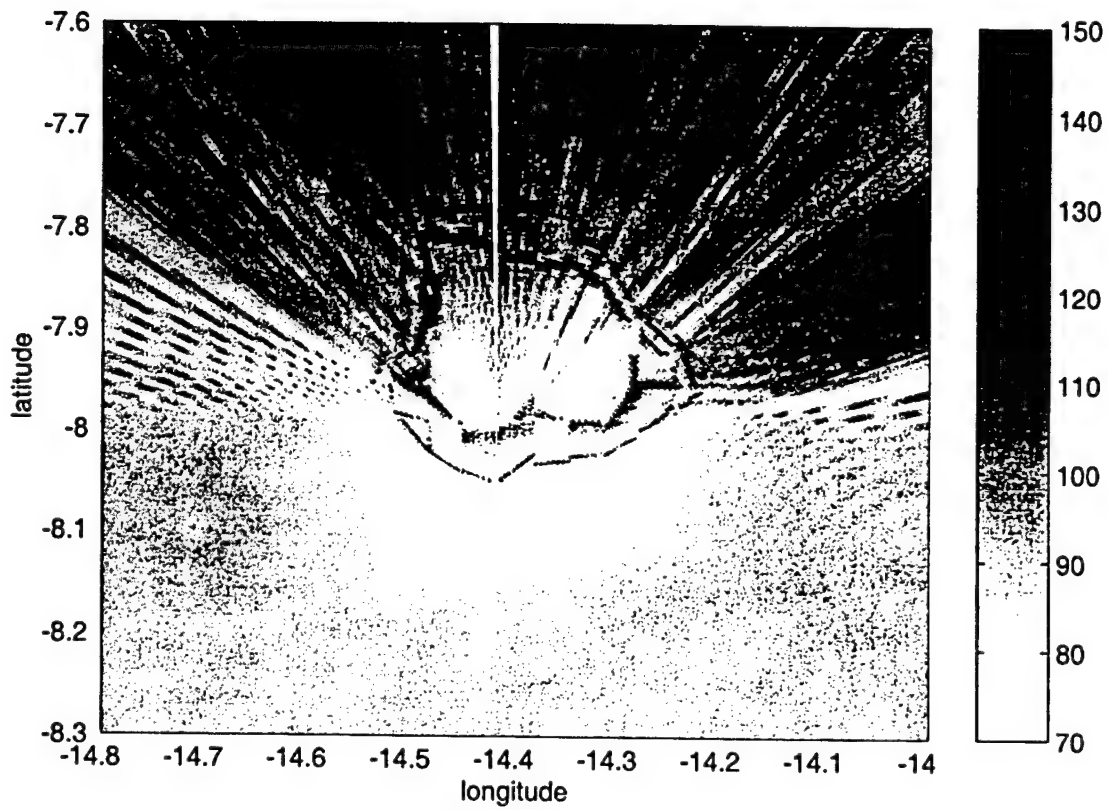
a) coarse bathymetry input.

Figure 12. Comparison of transmission loss computations at ASC24 for mode 3.
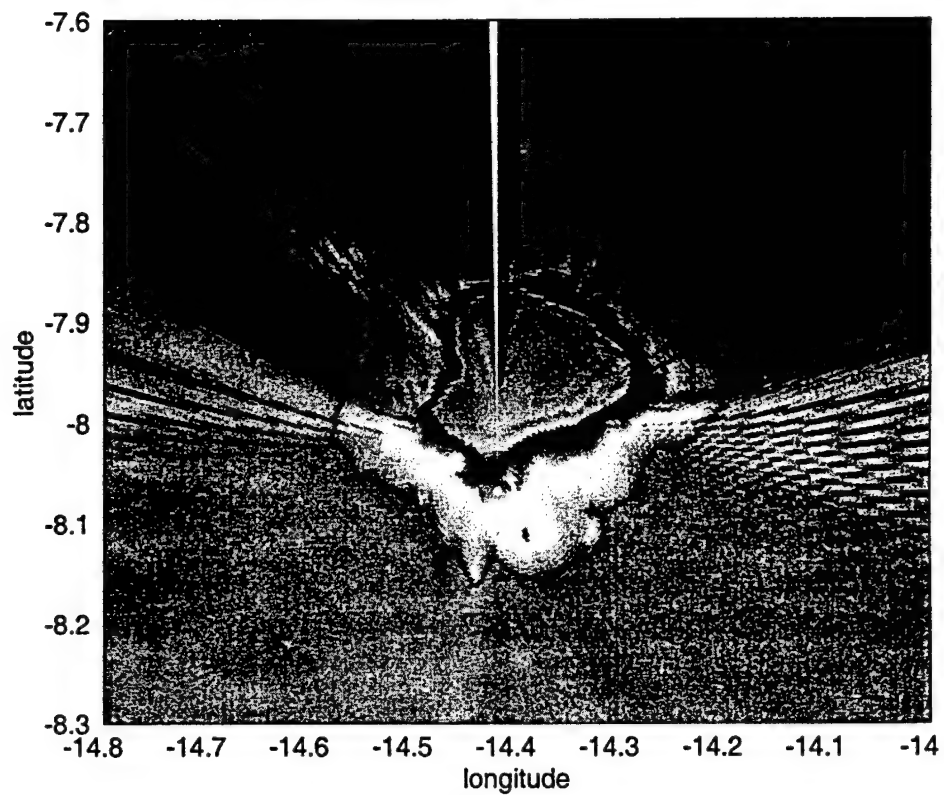
b) fine-scale bathymetry input.

Figure 12. Comparison of transmission loss computations at ASC24 for mode 3.
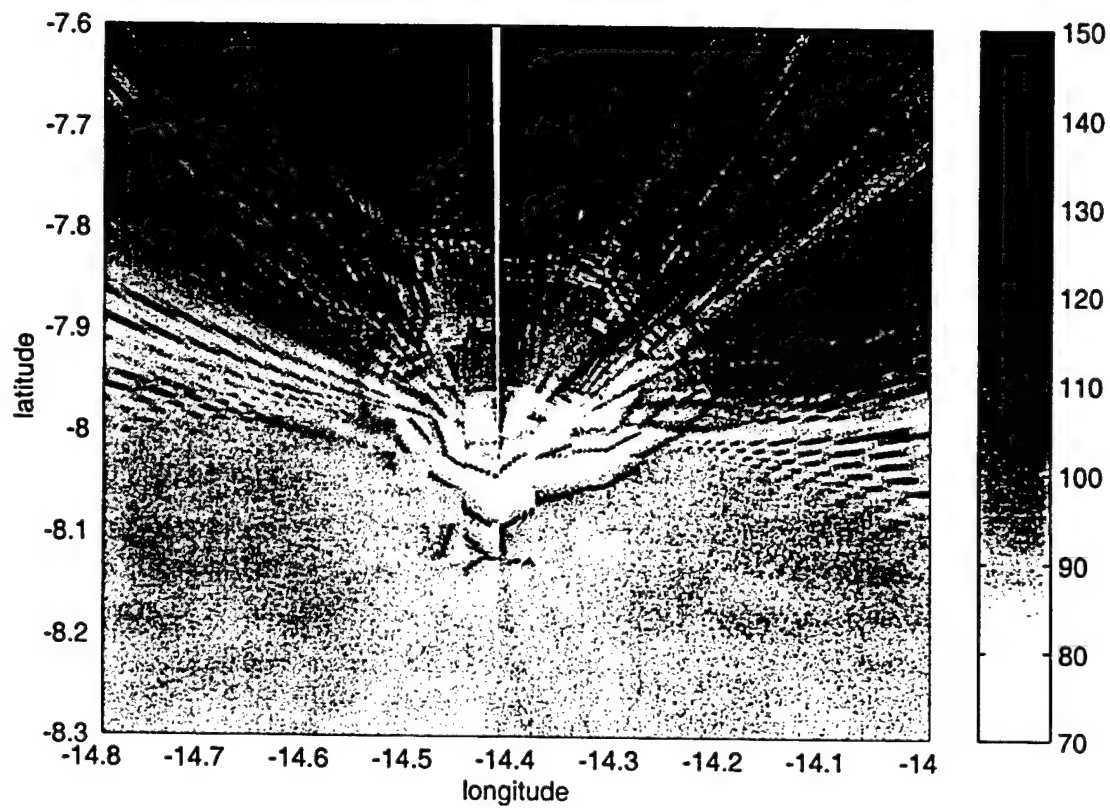
a) coarse bathymetry input.

Figure 13. Comparison of transmission loss computations at ASC24 for mode 4.
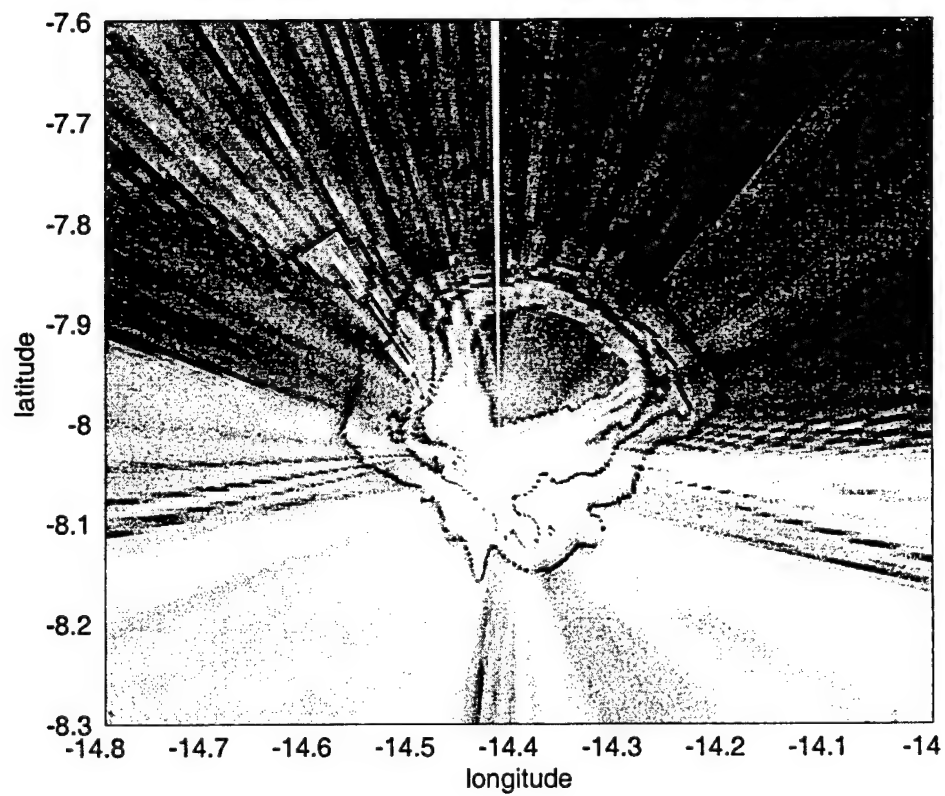
b) fine-scale bathymetry input.

Figure 13. Comparison of transmission loss computations at ASC24 for mode 4.

Section 3
Excitation of T-phases by Seafloor Scattering

T-phases excited by sub-oceanic earthquakes are classified into two types: abyssal phases which are excited near the earthquake epicenter at seafloor depths far below the SOFAR velocity channel, and slope T-phases which are excited at continental or ocean island slopes and ridges at distances up to several hundreds of kilometers from the epicenter. In this section, it is demonstrated that approximate time-frequency characteristics of both classes of T-phase can be synthesized under the assumption that T-phases are excited by scattering from a rough seafloor. Seafloor scattering at shallow depths preferentially excites low order acoustic modes that propagate efficiently within the ocean sound channel minimum. At greater depths, scattering excites higher order modes which interact weakly with the seafloor along much of the propagation path. Using known variations in near-source bathymetry, T-phase envelopes are synthesized at several frequencies for several events south of the Fox Islands that excited both types of T-phase. The synthesized T-phases reproduce the main time vs. frequency features of each type of arrival; a higher frequency, nearly symmetric arrival excited near the epicenter and a longer duration, lower frequency arrival excited near the continental shelf, with a peak amplitude at about 5Hz.

3.1 The Seafloor Scattering Model.

In this section, we show that, since seafloor scatterers excite acoustic modes in proportion to their intensities at the ocean floor, only leaky modes that interact with the seabottom can be excited. Scattering at shallow depths excites low order acoustic modes that initially propagate in both the ocean column and sedimentary layer, but cease interaction with the seafloor as they propagate seaward. Higher modes, which fill up more of the sound channel and are thus more prone to attenuation at seamounts and ridges, are preferentially excited at greater depth.

Given the significant velocity contrast between rock at earthquake source depths and the sediment covered seafloor, seismic energy is refracted nearly vertically upwards at the crust/sediment interface. Any method of numerically synthesizing the time-frequency characterisitics of earthquake-generated T-phases must account not only for the physics of coupling from nearly vertically propagating seismic waves to nearly horizontally propagating acoustic waves, but also the effects of seismic propagation through the attenuative crust and upper mantle, and acoustic transmission blockage by bathymetric features within the ocean column. As in de Groot-Hedlin and Orcutt(1999), we assume that T-phase excitation along the continental shelf is dominated by seafloor scattering, and that slopes are sufficiently gentle that acoustic propagation through the ocean waveguide is approximately adiabatic (*i.e.* we neglect mode coupling). If the seafloor is treated as a sheet of point scatterers, the pressure contribution from each point is given by the energy-conserving adiabatic mode solution to the wave equation in a stratified waveguide,*i.e.*,

$$p(r_r, z_r) = \frac{1}{\sqrt{|r_r - r_s|}} \sum_{m=1}^{\infty} \Psi_m(r_s, z_s) \Psi_m(r_r, z_r) \frac{exp(i \int k_m(s)ds)}{\sqrt{k_m |r_r - r_s|}} \tag{1}$$

(Collins, 1993), where $\psi_m(r_s,z_s)$ and $\psi_m(r_r,z_r)$ are the mode functions at the source and receiver locations, respectively, k_m is the complex wavenumber, and the summation is over the mode number m. For seafloor scatterers, the source depth is equal to the seafloor depth. Thus a point scatterer on the ocean floor excites modes in proportion to the mode amplitude at the ocean floor. Thus only leaky modes, that propagate in both the ocean column and the ocean bottom, can be excited by scattering of seismic energy into acoustic energy at the seafloor.

Energy is lost in the propagation of leaky modes as long as they interact with the seafloor. Given that k_m is complex valued, the exponential term in Equation 1 yields along path transmission losses. However, we chose instead to use a result from perturbation theory (Ingenito, 1973) to compute transmission loss; in this formulation, the attenuation of a given acoustic mode is estimated by the fraction of that mode's energy in the attenuative bottom. The total bottom attenuation along the transmission path from source to receiver is then given in dB by

$$dBloss = \beta f \int_{receiver}^{source} dr \int_{\infty}^{z_b} \Psi_i^2(z)dz, \qquad (2)$$

where β is the attenuation coefficient within the sedimentary layer, expressed in dB/km/Hz, and $z_b(r)$ is the bathymetric depth at any given horizontal location. Bottom losses thus trade off with energy excitation for any given mode and frequency. As seafloor depth increases, the attenuation of a given mode decreases and, at sufficient depths, the attenuation is negligible as the mode is transmitted entirely in the ocean column. An attenuation coefficient β of 0.10db/km/Hz was used, consistent with mean values for a sedimentary bottom (Biot, 1952).

The total pressure from the entire sheet of point scatterers is given by the summation over all points in the vicinity of the epicenter, $i.e.$,

$$\sum_{area} p(r_r,z_r)\left[\frac{e^{-d_s*\alpha*f}}{d_s}\right]^n s(\theta) \qquad (3)$$

where r_e is the epicentral location, z_e is the hypocentral depth, $d_s=[(z_e-z_s)^2+(r_e-r_s)^2]^{1/2}$ is the distance from the earthquake hypocenter to the seafloor scatterer, f is the frequency, α is the coefficient of attenuation within the crust and mantle, and $s(\theta)$ is the scattering coefficient as a function of the angle of incidence on the rough interface. The term in square brackets above describes the pressure incident from below on the rough seafloor, $i.e.$ pressure decreases due to spherical spreading and frequency-dependent attenuation within the crust and upper mantle. We use an α value of 0.02dB/km, consistent with mean values for oceanic crust (Hamilton, 1980).

The form of the scattering function and the frequency power law depends on the relative scale sizes of the scattering bodies and the wavelength of the sound energy. For scattering bodies that are small compared to the incident field wavelength, the scattered field can be approximated by the method of small perturbations (MSP), first used by Rayleigh (1894) to investigate scattering of sound at irregular surfaces. The MSP predicts that the intensity of the scattered field varies with the fourth power of frequency, $i.e.$ pressure varies as f^2, and that the scattered field is nearly omni-directional (Brekhovskikh and Lysanov, 1982). The tangent plane method, also called the Kirchoff approximation, is used for large-scale roughness. In this case it can be shown that scattered intensities are

27

independent of the sound frequency, *i.e.* n=0 in Equation 3. For the small slopes typical of sedimentary seafloors, it can be shown that the scattered field is concentrated in the specular direction (Brekhovskikh and Lysanov, 1982).

The seafloor is generally characterized by roughness over a wide range of scale lengths (*e.g.* Hertzfeld *et.al.,* 1995). For a rough interface with both small-scale and large-scale irregularities, it can be shown (Brekhovskikh and Lysanov, 1982) that scattering due to large-scale roughness dominates at low angles of incidence, and drops off rapidly with increasing angles. Scattering due to small-scale irregularities becomes more important at higher angles of incidence. However, since scattering by large-scale inhomogeneities directs energy in the specular direction, we conclude that it is no more efficient at generating T-phases than downslope propagation. In contrast, the scattered sound field excited by small-scale scatterers is nearly ommnidirectional; therefore we assume that, although only a small fraction of the total incident field is scattered, T-phases are primarily excited by small-scale scattering, for gently-sloping, sediment-covered seafloors typical of continental shelf regions. Thus, pressure amplitudes vary as f^2 and, since scattering strengths are only weakly dependent on angle of incidence, we set $s(\theta)=1$ in Equation 3 above.

A more complete description of scattering at a rough seabed, including the effects of non-zero shear velocities in the seafloor, as in Kuperman and Schmidt (1989), is beyond the scope of this paper. However, it should be noted that energy can only be scattered approximately in proportion to the S to P or P to P transmission coefficients. Thus, normally incident shear waves incident on the ocean waveguide cannot excite low grazing angle acoustic waves within the ocean waveguide. At higher angles of incidence, both P and S waves can excite T-phases, but the relative contribution will depend on the relative partitioning of P and S energy at the source, which is unknown. Furthermore, since the radiated energy depends on the size of the scattering bodies, which is unknown, we assume in this study that seafloor roughness is uniform over a broad region in the vicinity of the epicenter. Therefore, we do not specify an absolute value of the scattered energy, but seek only to demonstrate that small-scale scattering yields the general time-frequency characteristics of both slope and abyssal T-phases excited at a sedimentary seafloor.

3.1.1 Acoustic Excitation as a Function of Seafloor Depth.

The combined ocean/seafloor velocity profiles must be used to determine modal excitation at the seafloor. An acoustic velocity structure connecting an ocean velocity profile to a typical sedimentary seafloor P-wave velocity profile (Hamilton, 1979) is shown in Figure 14 for a water depth of 1km. The water column velocity profile was computed using an equation relating ocean temperatures and salinities to acoustic velocities (Mackenzie, 1981) for temperature and salinity data from the Levitus database (Levitus and Boyer, 1994). The seafloor can be treated as an acoustic medium, as S-wave velocities in the upper 100m of the seafloor are very low, on the order of 125m/sec (Hamilton, 1979, 1980) or even less. The first three modes corresponding to the velocity profile of figure 1a, computed using a WKBJ method (Jensen *et.al,* 1994), are shown in Figures 14b and c at 5Hz and 20Hz. As indicated, low order modes penetrate the ocean bottom at this depth and thus can be excited by scattering. At much higher frequencies, or greater depths, low order modes have zero amplitude at the seafloor, so they cannot be excited by seafloor scattering. Thus the modal excitation due to seafloor scattering depends on both frequency and seafloor depth.

28
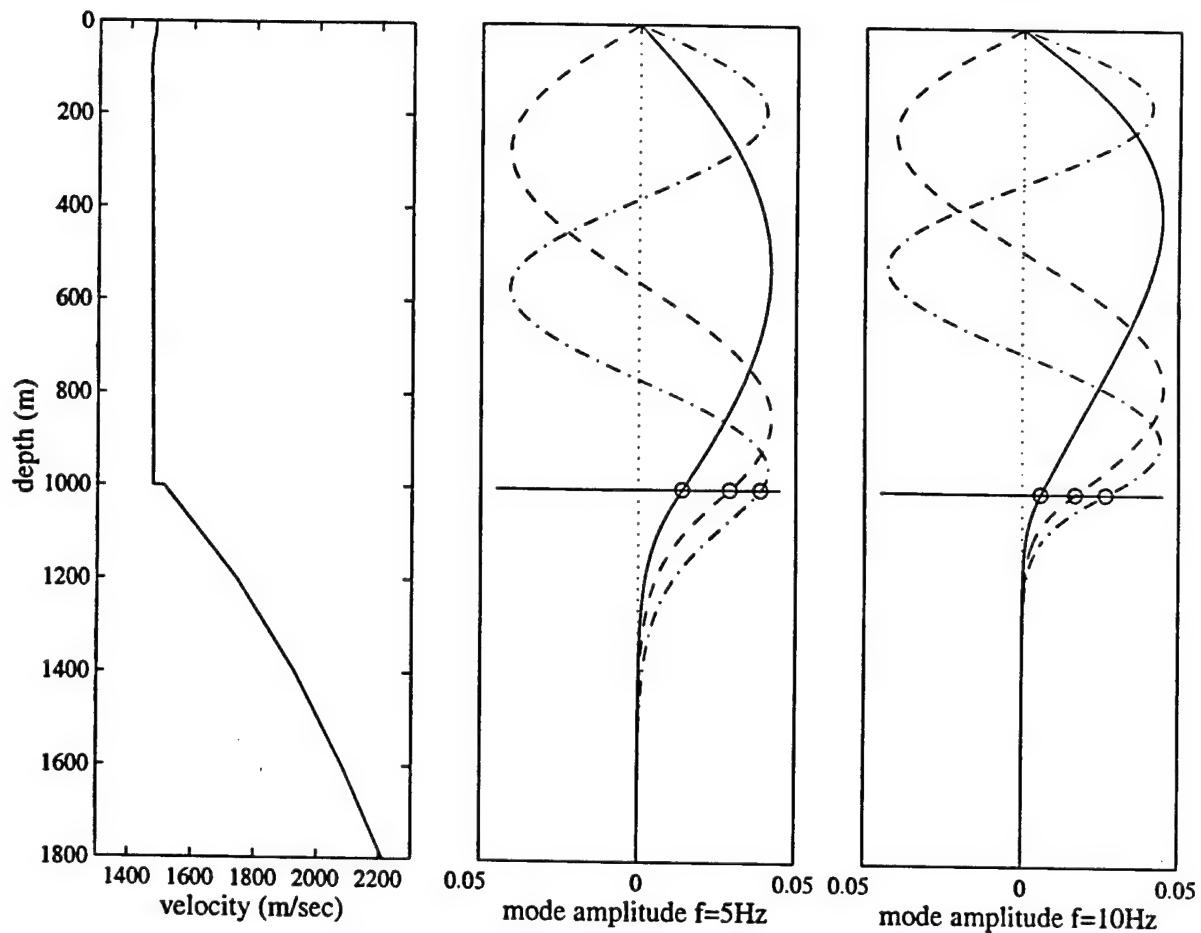
a) velocity profile used to compute acoustic modes for an ocean depth of 1 km. The top km. of the profile corresponds to annual average velocities near the epicenters; the bottom part of the velocity profile conforms to a typical seafloor sedimentary layer.

b) first three modes computed at 5Hz for the given velocity profile. Mode 1 is indicated by the solid line, mode 2 by the dashed line, and mode 3 by the dash-dotted line.

c) mode amplitudes computed at 10Hz.

Figure 14. Computation of modal excitation at the seafloor.

To estimate the modal excitation as a function of frequency and seafloor depth the computation indicated in Figure 14 was repeated for a series of frequencies and seafloor depths. At each depth, standard sedimentary seafloor velocity profiles were appended to ocean velocity profiles and mode amplitudes were computed at the seafloor. The mode intensity as a function of the seafloor depth, which we term the excitation function, is shown in Figure 15 for each of three modes and frequencies. As indicated, the excitation functions are strongly dependent on both frequency and depth. The optimal depth of excitation for any given mode increases with increasing mode number, and is approximately equal to the corresponding cutoff depth. Thus lower modes, which dominate acoustic signals at long ranges (Heaney *et.al.*, 1991), are preferentially excited in shallower regions. Further-
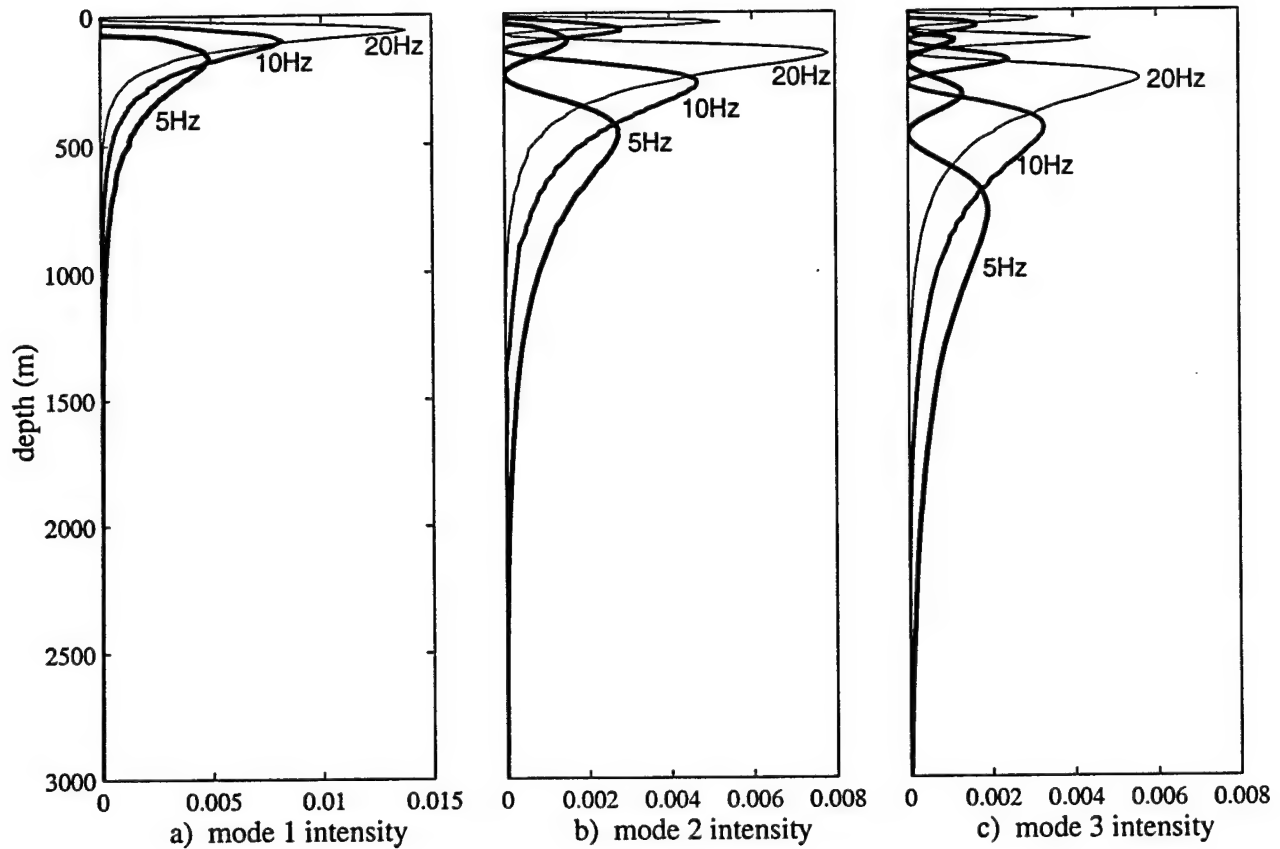
Figure 15. Acoustic energy excitation at the seafloor, as a function of seafloor depth, computed at frequencies of 5Hz, 10Hz, and 20Hz for annual average velocity profiles near the earthquake epicenters.

more, the peaks of the excitation functions decrease and become broader with increasing mode number, thus excitation of high modes is less efficient and less depth dependent than for low modes. Overall, this implies that the scattering of seismic to acoustic energy in shallow areas results in the excitation of low acoustic modes and that the strength of this coupling is strongly dependent on Furtherbathymetric depth. At a sloping interface, the acoustic energy in a given low mode ceases interaction with the bottom as it propagates into deeper water.

Modes excited by a point source on a flat seafloor at 4.5km depth are shown in Figure 16. Since a seafloor source can excite only bottom-interacting modes, lower order modes can be generated only at the lowest frequencies. As the frequency increases, only higher-order modes are excited. The corresponding transmission coefficients, *i.e.* the fraction of energy that is propagated to the receiver, are shown in Figure 16b for a path length of 4000km. As shown here, the transmission coefficients increase with frequency and decrease with mode number, reflecting the fact that higher modes and
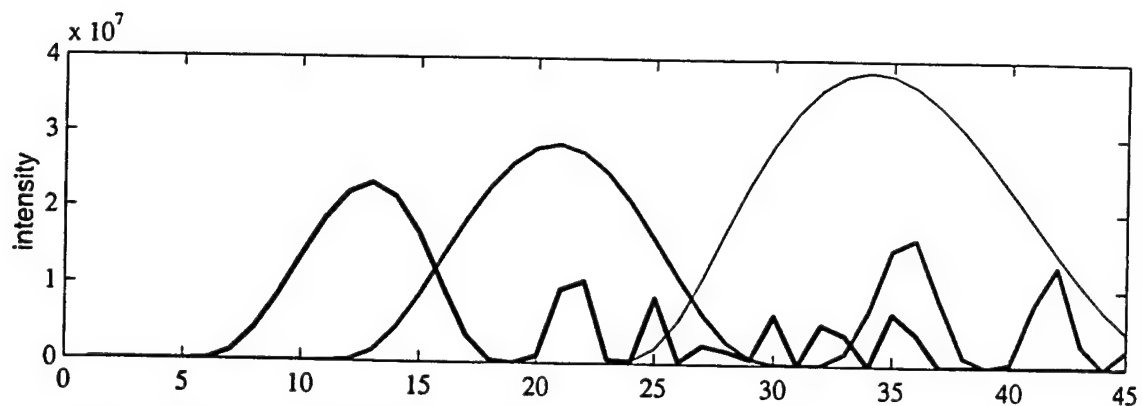
a) modal intensities excited at a seafloor depth of 4.5km for frequencies of 5Hz (thickest line), 10Hz (gray line), and 20 Hz (dashed line).
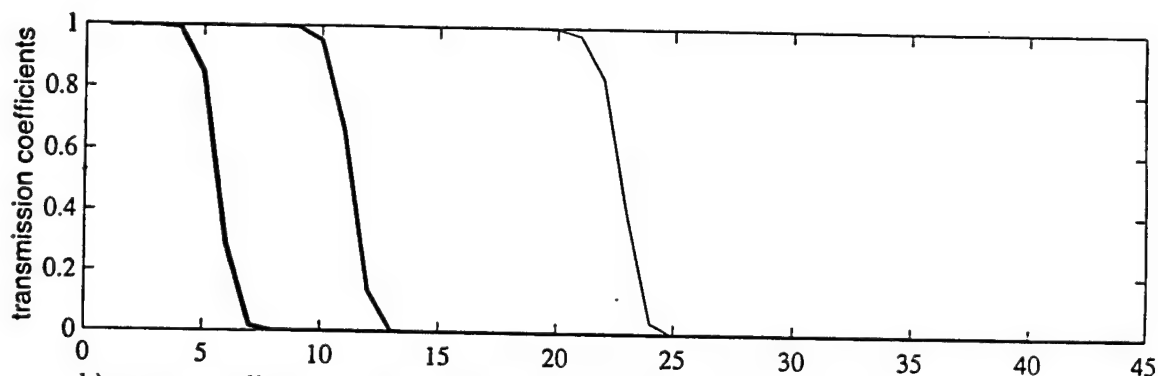
b) corresponding transmission coefficients for a path length of 4000km, for a flat seafloor at 4.5km depth.
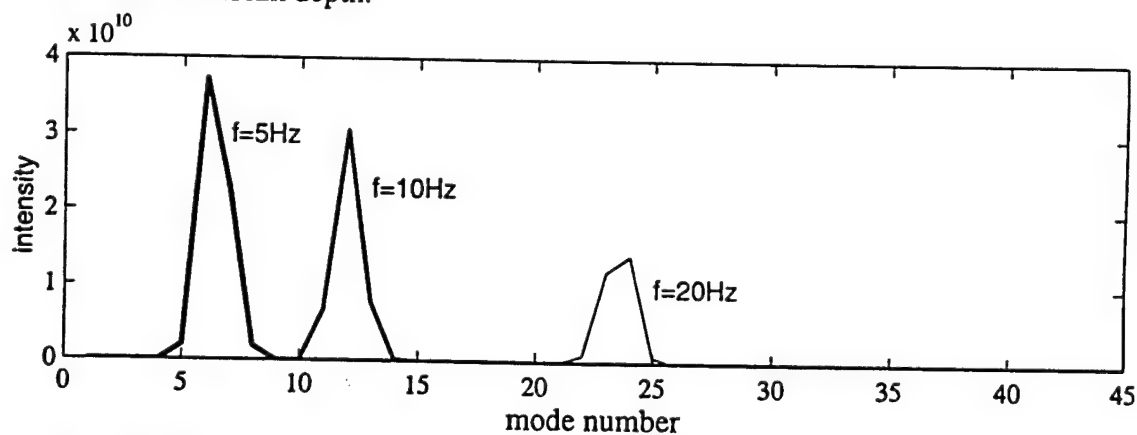
c) modal intensities observed at a receiver at a distance of 4000km, given by the products of values in Figures 16a and 16b.

Figure 16. Excitation of the abyssal T-phase

31
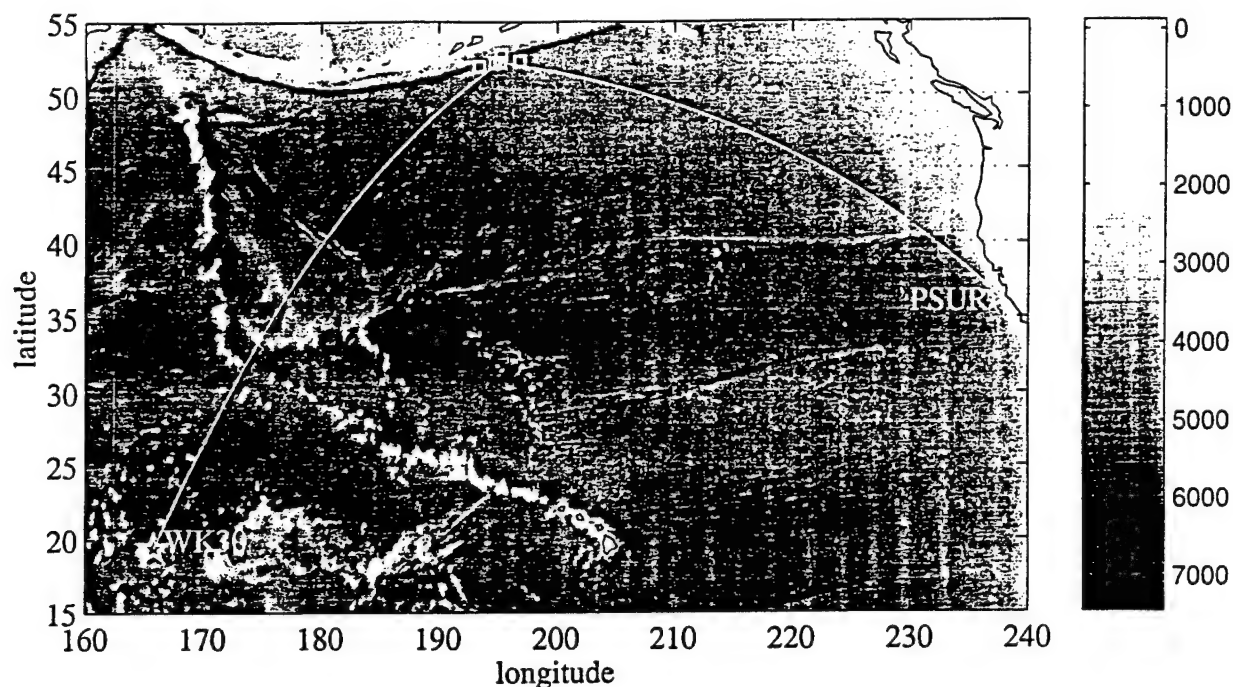
Figure 17. Bathymetry of the North Pacific Ocean. Locations of the Pt. Sur (PSUR) and Wake Island (WK30) hydrophones are marked by stars; epicentral locations are labelled by squares. Geodesic paths from one of the epicenters to each hydrophone are indicated by solid lines.

lower frequencies penetrate more deeply into the bottom. In general, the attenuation depends strongly on the bathymetry along the transmission path; higher modes are stripped away by bathymetric promontories. However, even for an ocean floor that is perfectly flat from source to receiver, higher order modes are stripped away with increasing source-receiver distance, as they interact with the seafloor along the entire transmission path. The modal energy observed at the receiver is a product of the modal excitation and transmission coefficients and is shown in Figure 16c. As indicated, the lowest modes excited at the epicenter are transmitted most efficiently. These are modes that interact very weakly with the bottom, thus are only weakly excited. At these depths, excitation is nearly independent of seafloor depth.

3.1.2 Computation of Travel Times.

Finally, acoustic travel times for each point are derived by integrating the modal group velocities along geodesic paths from each gridpoint to the receiver. The average seismic phase velocity for a cluster of events may be estimated by comparing the length of the seismic travel path to time delays between observed T-phase arrivals and computed acoustic travel times, as in the next section.

Several events south of the Fox Islands in the Aleutian chain excited both classes of T-phases which were recorded at hydrophones near Wake Island and off the coast of California. A map relating source and hydrophone locations is shown in Figure 17. A detailed map showing bathymetry and estimated epicentral locations is shown in Figure 18. As indicated, ocean depths at the epicenters
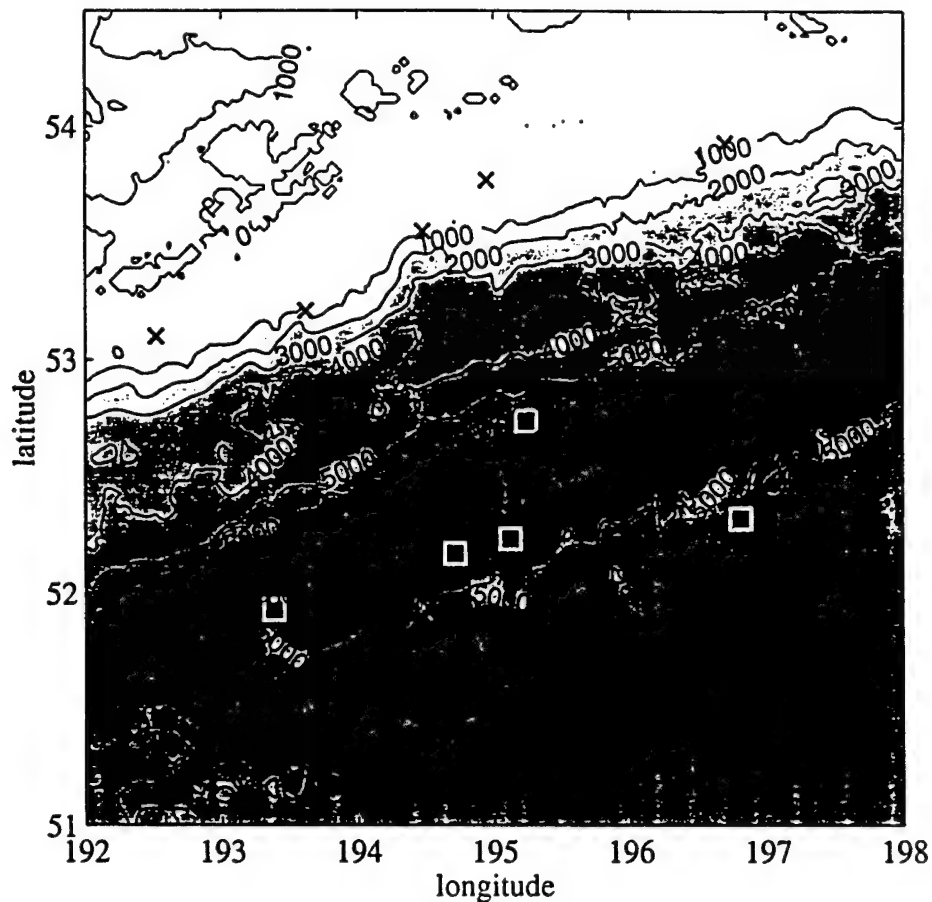
Figure 18. Bathymetry near the Fox Islands, in the Aleutian Chain. Epicenters for earthquakes that excited both slope and abyssal T-phases are indicated by squares; x's show the source locations for the associated high amplitude T-phase arrivals. Bathymetries are derived from satellite altimetry data (Smith and Sandwell, 1997).

range from 5 to 6km, far below the sound channel. Spectral ratio sonograms computed for the T-phase recordings at WK30 and Pt Sur are shown in Figure 19. For the WK30 recordings, each sonogram exhibits at least two arrivals, with the high frequency abyssal phase preceeding the lower frequency, longer duration, slope phase. A notable feature of the later arrivals is that their signal-to-noise ratios are greater than those of the abyssal T-phase although they' are generated further from the earthquake hypocenter. Also, the strength of the slope and abyssal T-phase arrivals near Wake Island are comparable, but at Pt. Sur the abyssal T-phases generally have much lower amplitudes than the slope phases, and are barely discernible for two of the events. This suggests that the abyssal T-phase is more susceptible to transmission blockage by bathymetric obstacles than the slope phase, consistent with our hypothesis that the abyssal phases are made up of higher order modes, which are susceptible to mode-stripping by bathymetric obstacles along the travel path.

Integration of modal group velocities indicates that modal dispersion along the source-receiver path

33
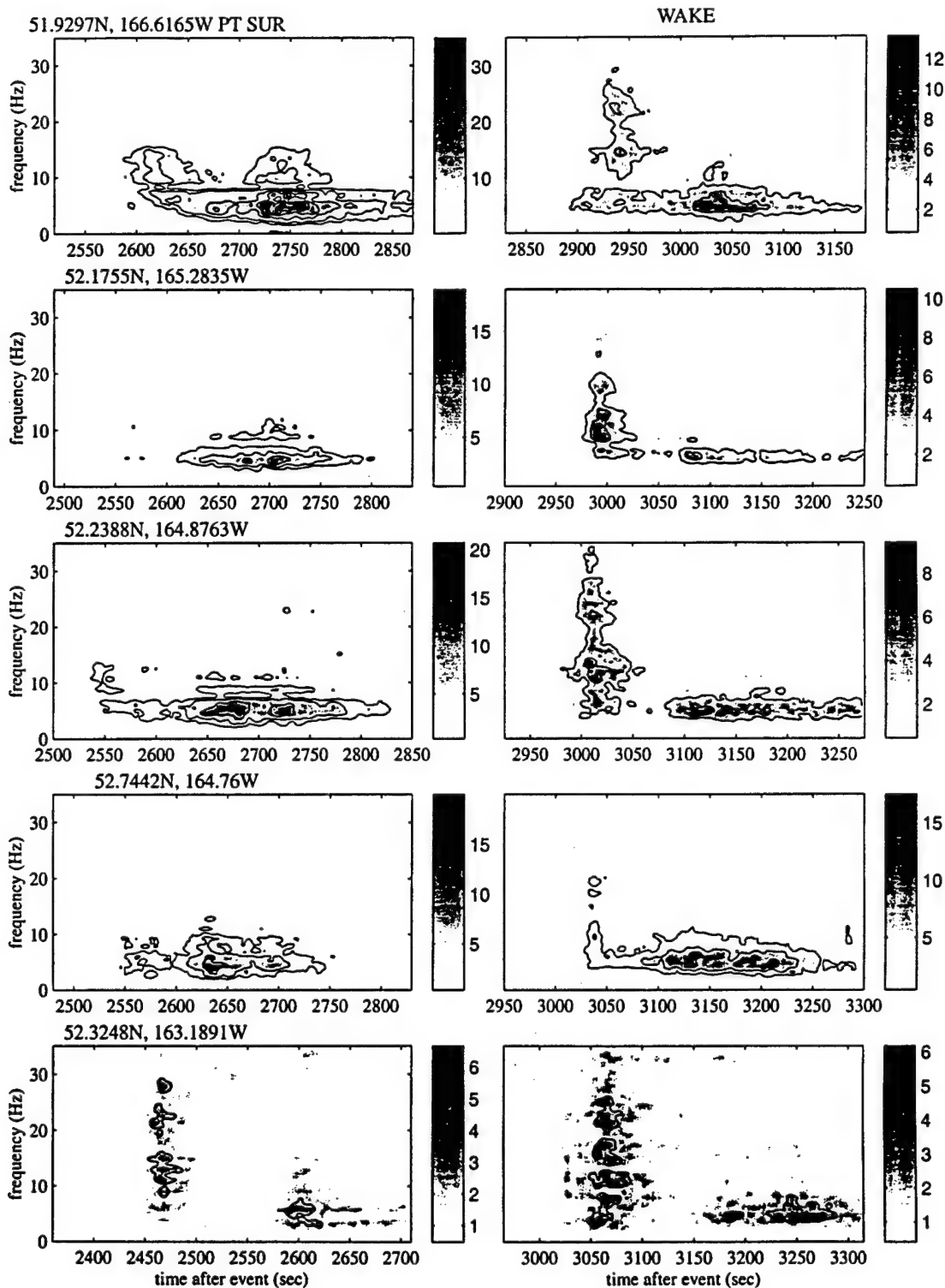
Figure 19. Spectral ratio sonograms for each recording at the Pt. Sur (left) and Wake (right) hydrophones, formed by dividing the power spectrum for each time slice by average noise powers computed for quiet intervals before the T-phase arrivals. Events are shown from west (top) to east (bottom); epicentral locations are given for each sonogram pair. Contours indicate signal to noise ratios at intervals of 3,6,12,18,24,30. Depth estimates are between 30 and 40km for all events.

34

is on the order of several seconds. This is negligible compared to the length of the T-phase wavetrains, and suggests that T-phases are generated over a distributed region of the seafloor. However, we define the T-phase source location as that corresponding to the peak arrival time, and estimate this for each phase. The total travel time for each phase is equal to the sum of the seismic travel time through the crust and upper mantle, and the acoustic travel time for oceanic propagation. The latter quantity is computed for a grid of points in the vicinity of the epicenter by integrating SOFAR channel velocities, derived from the WOA database (Levitus and Boyer, 1994), along geodesic travel paths. Since the seismic velocity, and hence the seismic travel times, are unknown, T-phase source regions are not uniquely identified. Therefore, given earthquake onset times and arrival times for each phase at only two hydrophones, the T-phase source locations are defined along arcs, which trend north-south for the given source-receiver geometry. Given additional reasonable assumptions about the seismic velocity - we assume that it must be greater than the average SOFAR velocity and less than 8km/sec- and given that observed T-phases cannot be generated where acoustic transmission is blocked along the source-receiver path, T-phase source locations can be pin-
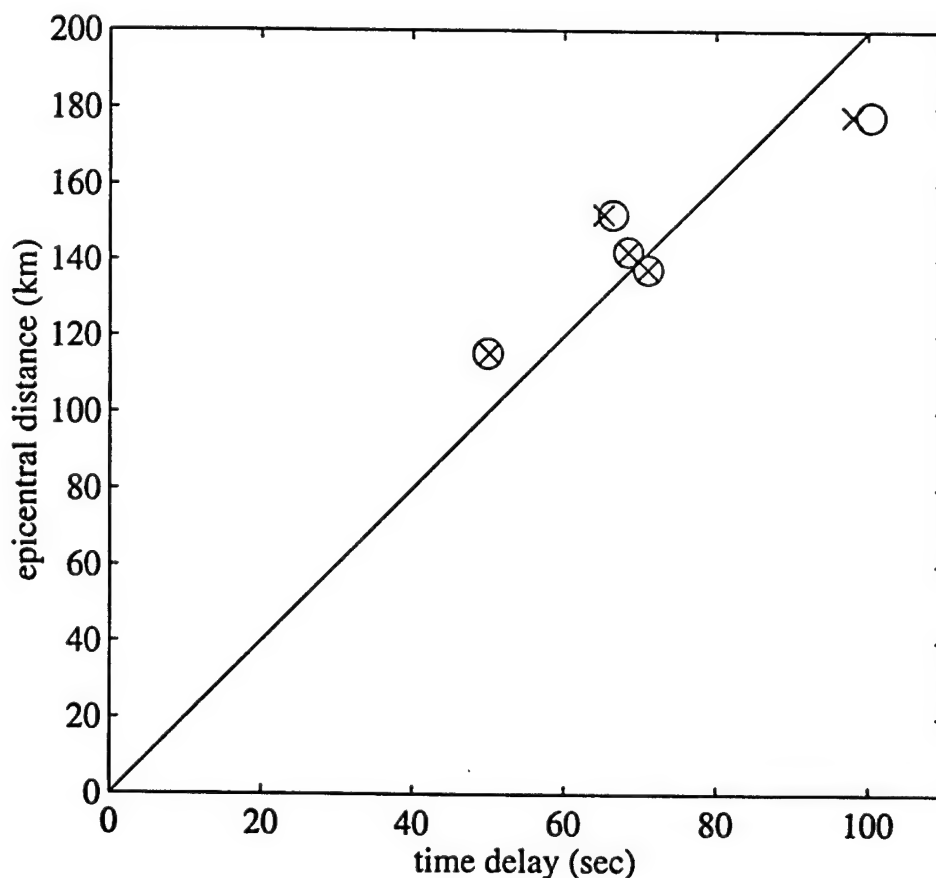
Figure 20. Hypocentral distance of the peak slope T-phase source location versus the seismic travel time through the crust and upper mantle, defined as time delay between the observed T-phase travel time and the computed acoustic travel times for the T-phase source. Circles indicate the seismic travel time derived for the Wake arrival, x'es indicate the corresponding value for Pt.Sur. The seismic velocity is given by the slope of the line, which is 2km/sec.

pointed to within 0.1 degrees in both longitude and latitude.

Source location estimates for the slope T-phases are also shown for each event in Figure 18. Abyssal T-phase source locations are coincident with epicentral locations to within the accuracy of the location estimates and time picks. The lower frequency slope T-phases are generated at greater distances from the epicenter, in regions of shallow, sloping bathymetry, in agreement with previous studies (Shurbet and Ewing, 1957; Johnson and Norris, 1968; Johnson *et.al,* 1968). The approximate linearity between the seismic delay times (defined as the difference between the T-phase arrival time and the acoustic travel time) and the distance between the epicenters and corresponding T-phase source locations gives us confidence that the T-phase source locations are accurately estimated. These values are plotted in Figure 20; from the slope we compute a velocity of 2.0 +_ 0.3 km/sec for the seismic phase coupling to the slope arrivals. The slow seismic velocity suggests that T-phases excited at large distances from the epicenter result from the conversion of shear waves to the ocean-borne acoustic phase.

The corresponding velocity of the seismic phase that couples to the abyssal T-phase is poorly determined, given the accuracy of the picks and of the estimated source locations. Given that only P waves can excite acoustic energy within the waveguide at normal incidence, the seismic velocity associated with the abyssal phase is likely greater than 2km/sec. However, given the short distance travelled by the seismic wave prior to conversion to an abyssal phase, this value is sufficiently accurate for our computations.

3.2 Numerical Examples.

Here we model T-phase arrivals at the WK30 hydrophone for several events south of the Fox Islands, using known variations in near-source bathymetry. Only arrivals at WK30 are synthesized, since instrument corrections are not available for the Pt. Sur hydrophones. We assume that the source rupture duration and area may be treated as a point source in both time and location. Furthermore, we assume that the source radiates seismic energy uniformly across the frequency band of interest.

Synthesized source regions for T-phases excited by the event at 52.1755N, 165.2835W, with a depth estimate of 37.5km are mapped in Figure 21 for several modes, at a frequency of 5 Hz. The pressure at each point is given by

$$\frac{1}{\sqrt{|r_r - r_s|}} \Psi_m(r_s, z_s) \frac{exp(i \int^{|} k_m(s)ds)}{\sqrt{k_m |r_r - r_s|}} \left[\frac{e^{-d_s * \alpha * f}}{d_s}\right] \psi^2. \tag{4}$$

As shown, T-phase energy in the lowest modes is excited along the shallow regions at the edge of the continental shelf. Areas to the western and northern ends of the source region are in an acoustic shadow, blocked by the Emperor seamount chain and by the Aleutian Islands, respectively. With increasing mode number, the T-phase excitation increases in the vicinity of the epicenter and decreases in the shallow areas. For yet higher acoustic modes, the acoustic energy observed at Wake becomes negligible due to mode stripping by bathymetric obstacles along the source-receiver path. Thus, the low modes, that are excited further from the epicenter, are associated with the slope T-phase. Higher modes, excited nearest to the epicenter, are associated with the abyssal T-phase. At

36

higher frequencies, the incident energy at the continental shelf decreases due to the frequency dependent attenuation of the seismic phase, so the slope phases are only weakly excited.

The synthesized mode envelopes for this event, formed by summing arrivals within two second bins, are plotted in Figure 22 as a function of time after event rupture for several frequencies. T-phase energy excited in the shallow regions is concentrated in lower modes and has greater duration than the T-phase energy excited in the epicentral regions. The abyssal phases appear in the higher modes, and are nearly symmetric about the peak amplitudes. The separation of "slope-generated" T-phases in the low modes, and the abyssal energy in the high modes, becomes more apparent with increasing frequency. Note the decrease in amplitude of the slope T-phase compared to that of the abyssal T-phase at the higher frequencies, due to the greater attenuation of seismic energy in the
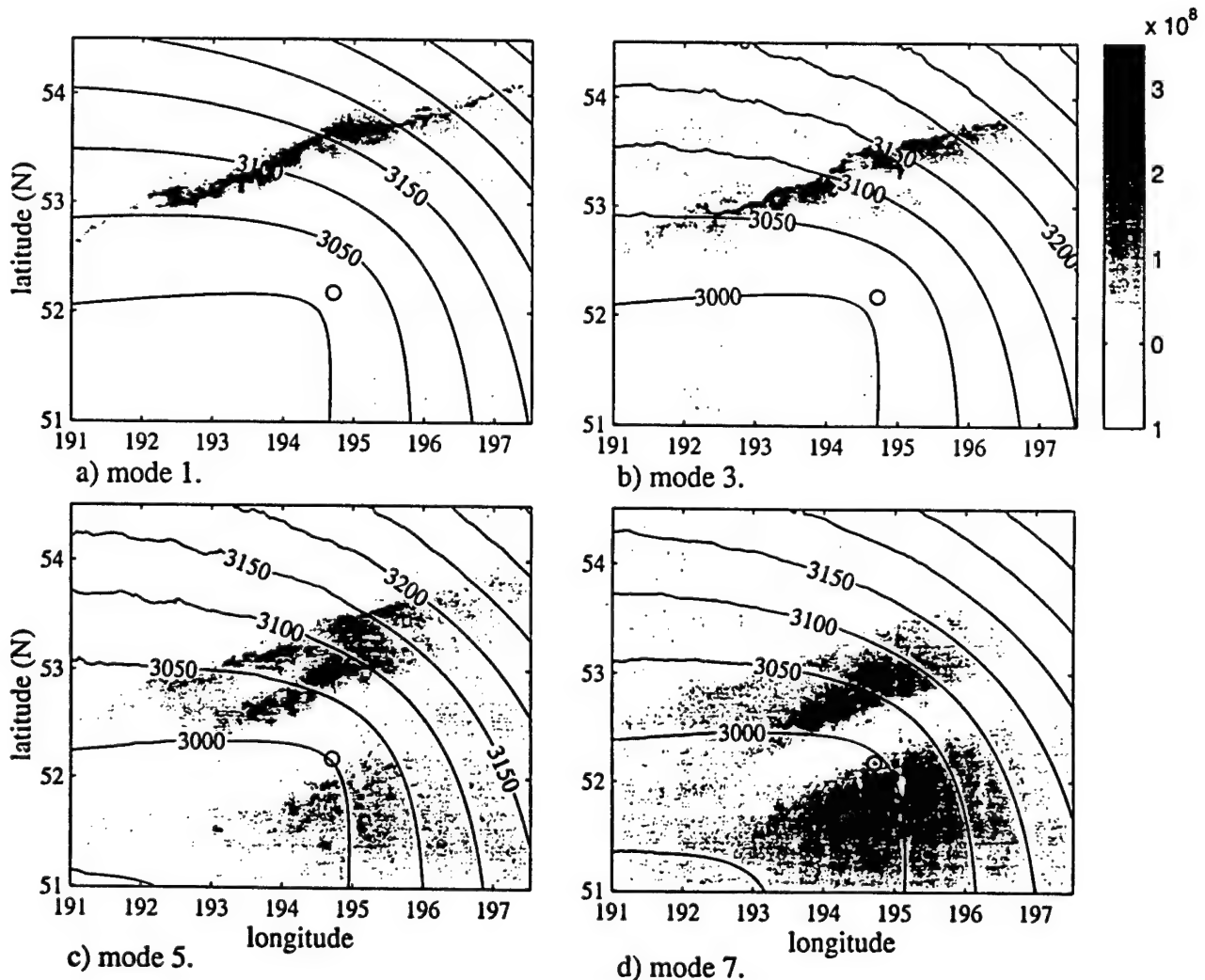
Figure 21   Acoustic source regions for T-phases observed at WK30, for several modes at a frequency of 5 Hz. Dark areas indicate areas of greatest T-phase excitation. All plots are shown to the same grayscale. The epicenter is marked by a white circle. Superimposed contour lines show the T-phase travel time in seconds after the earthquake.

37
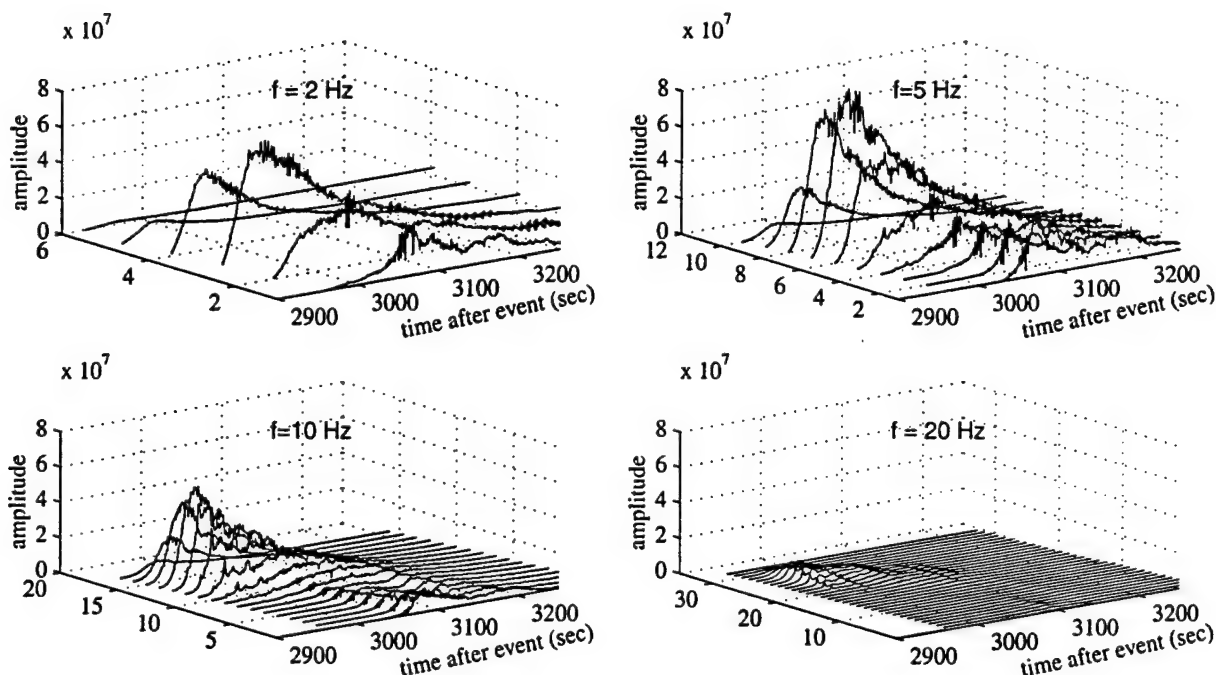
Figure 22. Computed acoustic T-phase envelopes for a range of modes at several frequencies for an event at 52.1755N, 165.2835W, at a depth of 37.5km.

crust and upper mantle.

Envelopes were formed at frequencies of 2,5,10, and 20Hz by summing intensities at each mode, weighted by the mode functions at the receiver locations. Finally, the synthesized sonograms were formed by linear interpolation between the envelopes; these are shown in the left column of Figure 23. The real, instrument corrected sonograms are shown to the right. Sonograms are shown only for four of the events shown in Figure 19; the center one, at 52.2388N, 164.8763W was left out due to its proximity, hence its similarity to the event at 52.1755N, 165.2835W.

Although not a perfect match, several characteristics of the synthetic sonograms agree with corresponding features of the WK30 sonograms. Both real and synthetic slope phases, which trail the abyssal phases, show a peak in energy at about 5Hz, and have longer duration than the abyssal events. The synthetic sonograms also correctly predict that the abyssal T-phases have higher frequency content than the slope phase, and are nearly symmetric about the peak amplitdes. Arrival times for the abyssal phases agree, with the exception of the third event, which had a poorly connstrained location. However, the computed abyssal phase has too low a dominant frequency, and falls off too rapidly with incresing frequency. Discrepancies between real and computed sonograms may be due to the simplifying assumptions made in the modeling, as discussed in the next section.

38
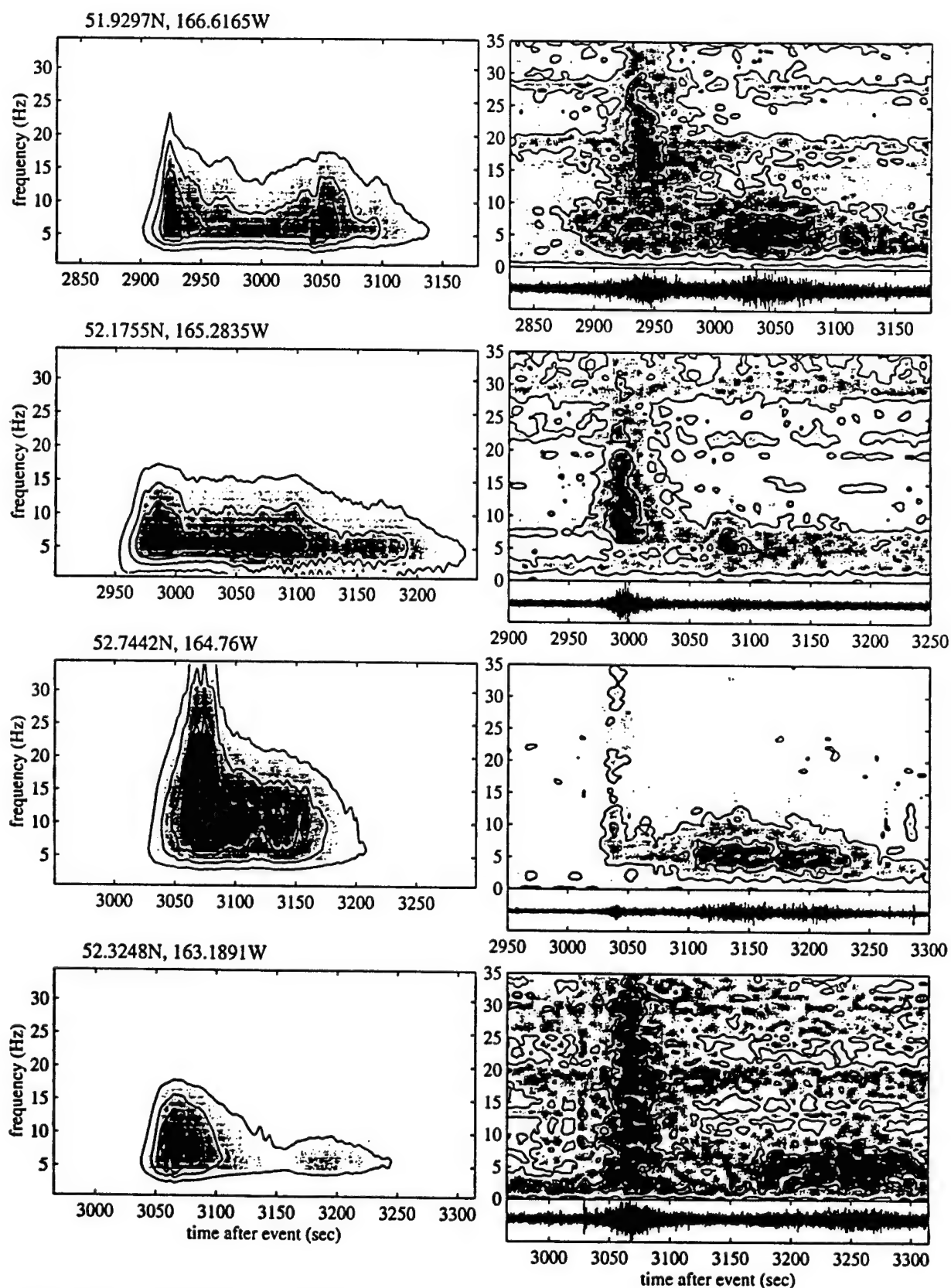
Figure 23. Comparison of synthetic, left, and real sonograms, right, recorded at WK30. Recorded waveforms, bandpassed from 2-20Hz are also shown. The epicentral locations used in computing synthetics for each event are given.

3.3 Discussion.

A number of simplifying assumptions were made in the synthesis of the T-phase envelopes in order to isolate the effects of seafloor scattering from other geophysical effects. As a result, variations in amplitude with frequency and the relative scale sizes of the abyssal and slope phases are poorly constrained in this analysis. Factors which affect the frequency dependence of the observed T-phases are the earthquake source spectrum and the scale size of the seafloor scatterers. We have make the assumption that the characteristics of the seafloor near the Aleutian trench are similar to those of the continental shelf region. Furthermore, our assumption that the earthquake source spectrum is flat over the entire frequency range is true only if both the fault rupture surface and rupture duration are infinitesimally small (Aki and Richards, 1980). For more realistic sources, the frequency spectrum drops off approximately as 1/f for frequencies greater than about 1Hz; this makes the excitation of higher frequencies even more problematic.

Factors which affect both the variation in T-phase amplitude with frequency and the relative amplitudes of the slope and abyssal T-phases are the seismic attenuation coefficients (α and β), the source depth, and the bottom velocity profile. An increase in β, the seismic attenuation of the sedimentary seafloor, results in a decrease in the abyssal T-phase amplitude relative to the slope phase since the abyssal T-phase interacts with the seafloor along a much greater portion of its propagation path. However, increasing α, the attenuation coefficient for the upper mantle and lower crust, decreases the computed amplitudes of both the slope T-phase and the high frequency abyssal T-phase since the loss is proportional to the number of wavelengths traveled by the seismic phase through the crust and upper mantle. Unfortunately, although the frequency dependence and relative amplitudes of the slope and abyssal phases are strongly dependent upon the value of the seismic attenuation coefficients, these values are only approximately known, so that only order of magnitude computations can be done. Furthermore, shallow sources are predicted to be associated with high amplitude abyssal phases with higher dominant frequencies than deep sources, given the shorter seismic travel path through the attenuative crust and mantle. Finally, the velocity gradient within the seabottom affects the mode functions, and hence the computed amplitudes. For a high velocity gradient, the mode functions decrease rapidly with depth so the propagation loss due to seafloor interaction decreases. The effects of decreasing the velocity gradient is thus similar to increasing the attenuation coefficient β, *i.e.* it decreases the computed amplitude of the abyssal T-phase.

An unexpected result of our analysis is that, although shear wave velocities in the sediments are so low that the seafloor may be treated as a fluid in computing the mode functions, the velocity of the seismic phase coupling to slope T-phases is consistent with shear waves. A mechanism to resolve this apparent incongruity is that S-waves convert to compressional waves at the interface between the elastic, oceanic crust and the seafloor sediments; this is supported by observations (Spudich and Orcutt, 1980) that shear waves are converted at the sediment-rock interface and not at the sediment-seawater interface. Computations of S- and P- energy flux densities at the crust-sediment contact indicate that, at high angles of incidence, crustal shear waves impinging on the sediments are mainly refracted into the sediments as acoustic energy. At low angles of incidence, the shear waves are mainly reflected back into the crust. Compressional waves are mainly reflected back into the crust at high incidence angles, with a smaller portion refracted into the sediments. In this case, the abyssal phase is more likely to result from the conversion of P-waves and the slope phase from the transfor-

Section 4

Seismoacoustic Detection of Events in the Norwegian Sea

The U.S. Navy North Atlantic hydrophone arrays were installed during the cold war for tracking submarines. The decline of the Soviet Union and budgetary considerations led the U.S. Navy in the early 1990's to allow limited access to the acoustic data for scientific studies (Fox et al., 1994; Nishimura and Conlon, 1994). In 1995, NRL established a system to archive data from North Atlantic arrays that recorded 16 channels of beamformed data. The beamforming was accomplished by Navy hardware using an adaptive approach tuned for arrivals traveling at the speed of sound in seawater. We archived data from more than one array and chose the beams recorded on the 16 channels to emphasize acoustic arrivals from the Mohns Ridge and its intersection with the Jan Mayen transform fault. This was known to be an active portion of the plate boundary in the Norwegian Sea (Vogt, 1986; Figure 24). The most useful data in our archive covers the period from mid November, 1995, through September, 1996. This portion of the archive now resides at Scripps Institution of Oceanography in a classified facility at the Marine Physical Laboratory on Point Loma. The rest of the archive is at the Naval Research Laboratory in Washington DC and Clyde Nishimura was our main contact there throughout the study.

Our original intent to develop a publically available seismic and hydroacoustic waveform database for the project turned out not to be feasible since the hydrophone array data has not been cleared for large-scale release. During this project, only specific few-minute sections of the data were cleared, in non-digital form, for publication/presentation. The data would be available for future research but only to individuals with security clearance. The archive is on tape media so the lifetime is limited if no subsequent re-recording is done (none is currently planned).

The most commonly observed phase in the hydrophone data is the T-wave. Body waves are also recorded by the hydrophone arrays although these phases are less common than the T phase. Both P-waves and S-waves converted to an acoustic phase at the seafloor are seen for some regional events in the Norwegian Sea. For large teleseismic earthquakes P-waves were also recorded.

The most exciting outcome of the study was that we observed an episode of spreading on the Mohns Ridge in 1995. This was the first time that fairly detailed recordings of such activity had been obtained at an ultra-slow spreading center. Thousands of events ranging in magnitude from less than 1.0 to 4.8 mb occurred throughout a region about 20 km by 60 km in size. Below we highlight the character of these events and our ability to constrain their location. More detailed presentation is available in Blackman et al. (2000).

The level of background noise varies considerably throughout the study period. Whales intermittently contribute signals in the 17-22 Hz range and occasionally these are quite loud suggesting the mammal is close to a given array. More disruptive, though, are the seismic refraction/reflection shots that occur for longer duration and over many days throughout the period. In other parts of the ocean, these signals might not be guided as well by the sound channel but, particularly during the Winter months, the near-surface nature of the low velocity guide results in the shots being quite energetic even a fair distance from the source. Earthquake arrivals can be detected during these

41
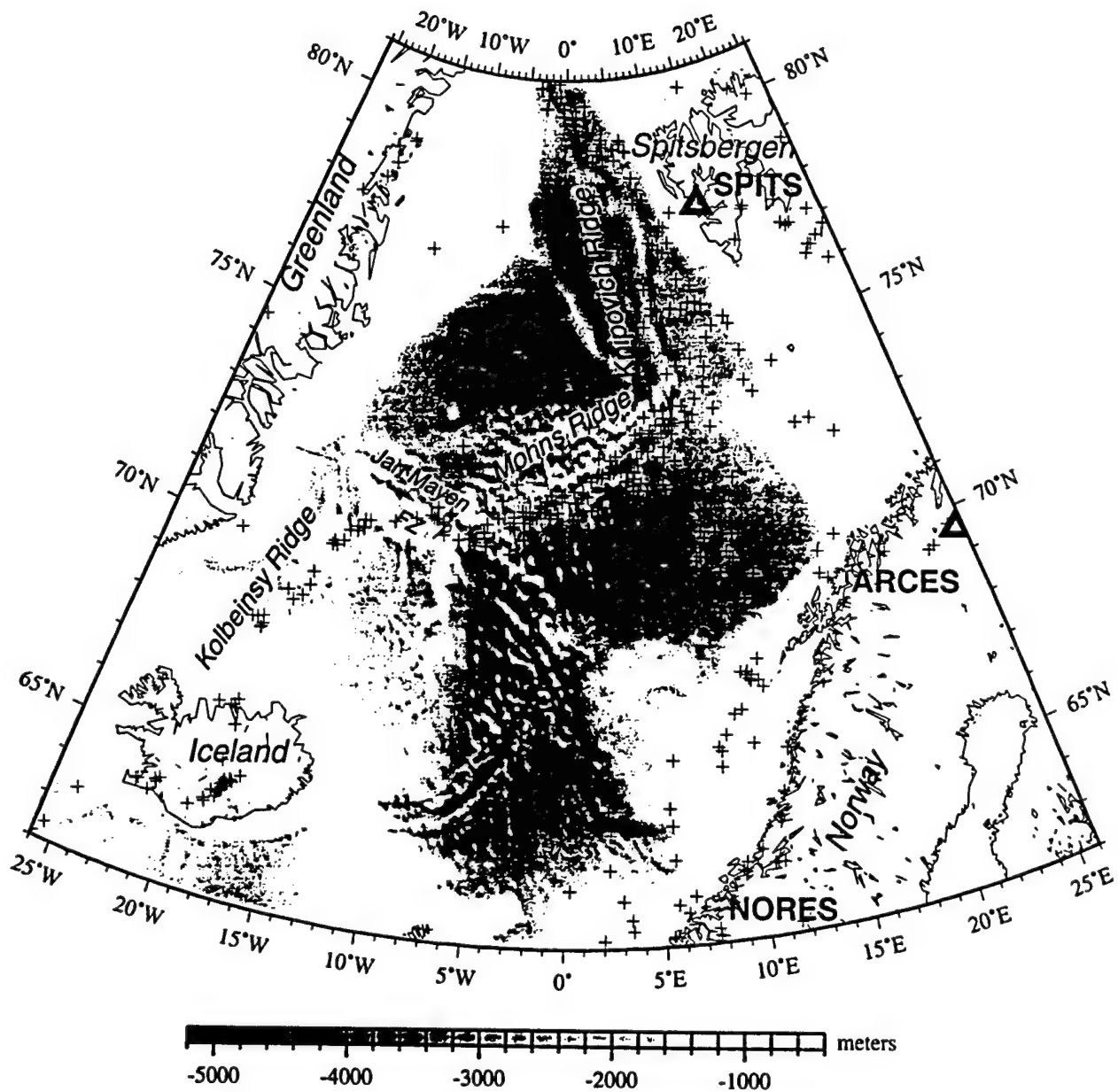
Figure 24. Regional map of the Norwegian Sea. Shading shows the topography with lighter shade for shallow depths and land. The three spreading centers are labeled and the Norwegian seismic arrays are indicated by triangles and bold labels. Earthquake epicenters listed in the REB for 1995-1998 are shown by +'s and most seismicity occurs along the plate boundary.

42

shooting intervals but arrival time picks have greater uncertainty and for very small events they cannot be made. Another source of noise is the swarm of earthquakes generated during the spreading episode as multiple events put significant energy into the water column and it reverberates for a finite time.

The early part of the spreading episode was marked by seven earthquakes of magnitude 3-4 and reported in the REB to occur on the Mohns Ridge 72°-72°30'N, 3°-6°E (Figure 24) over a period of
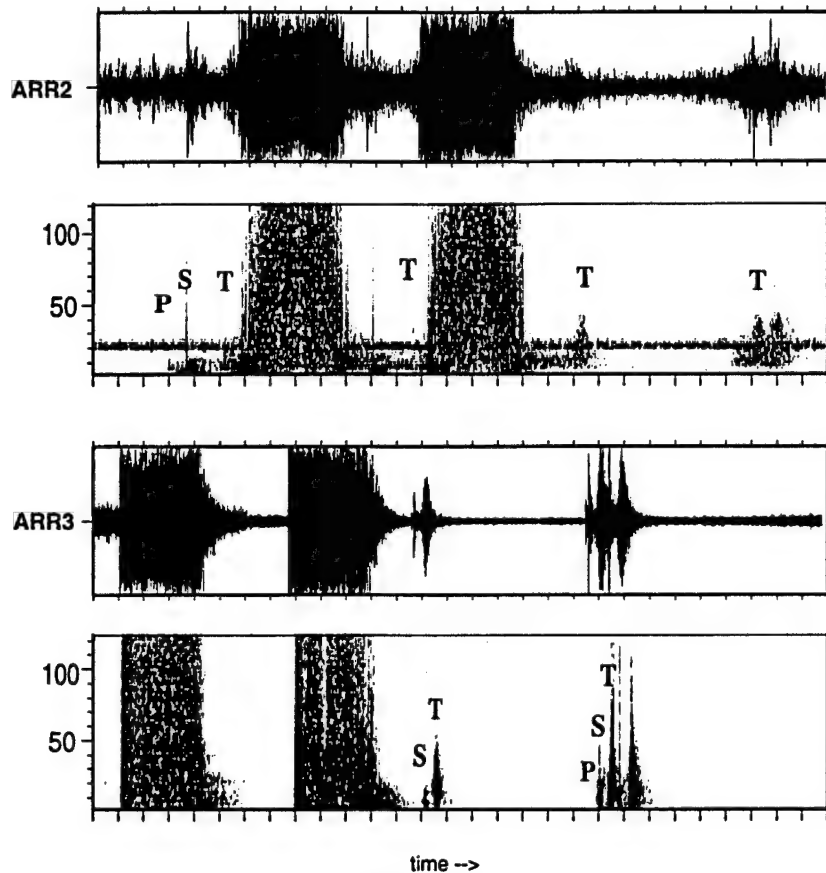
time -->

Figure 25. Hydrophone array recordings of a 3.5 mb event that occurred on the Mohns ridge in Nov95. Unfiltered time sections from single beams formed at Arr3, the closest array, and a representative more-distant array, labeled Arr2. The section is several minutes long. Corresponding spectra are shown for the same time sections. The arrivals from the first event are clipped at Arr3 but the body-waves for this event are visible in the spectrogram for Arr2. The T-waves are clipped for both of these larger events but 2 subsequent, smaller events show P, S and T arrivals at Arr3 and T-waves at Arr2. The consistent ~20 Hz signal on Arr2 is a whale.

43

five days in late November, 1995. A total of two dozen events were located by CMR in the same area for the period July, 1995, - January, 1996, with 19 of them occurring between November 27, Julian Day (jd) 331 and December 15 (jd 349). Ten events, including the largest (4.8 mb), were reported by CMR on jd 341-342 and activity detected by the onshore seismic arrays dropped off sharply after this time. The hydrophone data contain almost three orders of magnitude more record-ings of events during the swarm period than are listed in the REB, which represents only reasonably well-constrained seismic event locations. Most of these acoustic events are quite small judging from the relative amplitudes of the 2.8 ML - 4.8 mb events recorded onshore (and often clipped on the hydrophone array data) and the bulk of the arrivals from other events (Figure 25). P- and/or con-verted S-waves are recorded by at least one array for about 25% of the swarm events.

For sources in the Norwegian Sea, the seismic arrays NORESS, ARCESS and SPITS record Pn, Sn and an occasional T-wave that converts from an acoustic to a seismic phase at the continental slope and propagates to the station. Pn and Sn have the greatest energy in the 1-8 Hz range whereas the converted T-wave has lower amplitudes in mainly the 1-3 Hz range. In general, the SPITS array records shear wave arrivals from central Mohns Ridge events with very low SNR, and energy mainly below 2 Hz. Vertical component records from ARCESS stations, on the other hand, show Sn amplitude and frequencies similar to Pn for the same events. It is not clear where such shear-wave attenuation occurs but the most likely candidate would be beneath the Knipovich Ridge. When a spreading episode event was large enough to be reported in the seismic bulletin the hydrophone data usually showed a series of distinct events that occur over a few-minute period (Figure 26).
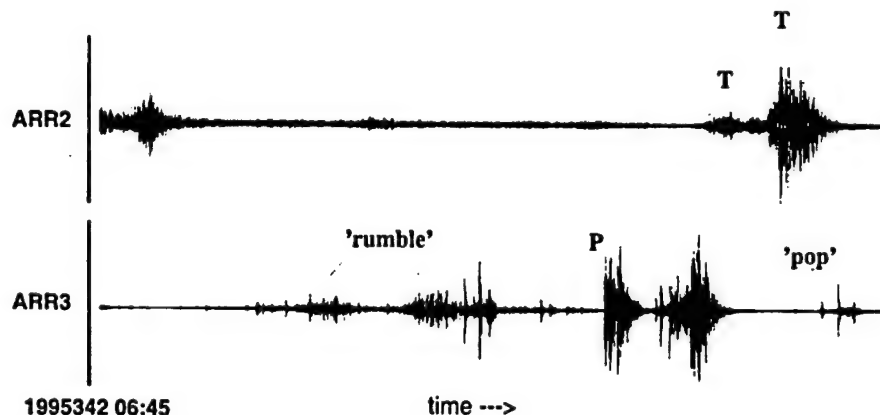
Figure 26. Example of occasional 'rumble' that occurs around the time of the most intense activity, jd 341-342. Several small 'pop' events are shown as are 2 earthquakes just large enough for the body-waves to clip. A single beam from Arr2 is shown for a few-minute period and the same period is shown for a beam from Arr3.

Two means of locating the swarm events were used with the hydrophone data. Many more events were recorded only on a close array than were recorded with high SNR on multiple arrays. For these events, relative event location were determined from changes in arrival time differences between T-, converted S- and P-waves. Since no additional constraint is available for these locations, we simply chose a reference point on the arc from the receiver that corresponds with a morphologic feature that is a likely locus of spreading activity: one of the axial volcanic highs. One of the CMR epicenters could be used as the master event for these relative location determinations but it appears that prior to 1997 (when SPITS data began to be routinely included in the analysis) there was a systematic bias towards the southeast in CMR locations in the central Norwegian Basin so we prefer a 'master event' within the rift valley. When T-waves are also pickable at more distant arrays we triangulate to a position with uncertainty on the order of 10-20 km depending on the T waveform. The T picks are made at the time of highest amplitude and frequency content within the broader arrival. None of the multiply-detected events can reasonably be located more than a couple tens of kms down the southeast flank of the ridge and they could all be within the rift valley (or perhaps somewhat to the northwest).

Section 5
Conclusions

Development of an Accurate Ocean Model.

Seasonal variations in modal group velocity can reach up to 4mm/sec, which could translate to a time difference of 9 sec. over a 5000km path. This is only a small source of error compared to the large errors routinely made in picking T-phase arrivals from earthquakes.

Comparison of global scale transmission losses at f=5Hz indicates that, overall, the higher resolution Smith and Sandwell bathymetric data yield wider and deeper shadow zones behind islands than the more coarsely gridded ETOPO5 data. Further results show that the differences in transmission losses increase with increasing mode number. This is to be expected since bottom interaction increases with increasing mode number, thus greater accuracy in the bathymetric database is required for higher mode numbers.

Excitation of T-phases by Seafloor Scattering.

We demonstrated that scattering of seismic to acoustic energy at a rough seafloor yields the approximate time-frequency characteristics of T-phases excited both at shallow regions within the SOFAR channel, as well as at depths far below the sound channel. This is consistent with the results derived by Park and Odom (1999) using a scattering formulation. The modeling predicts that, although T-phases are generated most efficiently at shallow depths, significant T-phase energy can be excited at depths of several kilometres. The abyssal phases consist of high order acoustic modes that interact weakly with the sediment layer along all, or almost all, of the transmission path but can have significant amplitude for paths with few bathymetric obstacles along the transmission path. For T-phase excitation distant from the epicenter, shear wave energy transforms to low order acoustic modes at bathymetric promontories. The abyssal phase results from direct conversion of P-waves to higher order acoustic modes. For both the slope and abyssal phases, the scattered energy correspond to rays that initially have grazing incidence on the seafloor; as depth increases, the slope "rays" become entrained within the sound channel minimum. The model predictions agree with the observations (D'Spain *et.al,* 1999) that sources within the sofar sound channel excite low mode energy, whereas sources far below the channel excite higher acoustic modes.

Seismoacoustic Detection in the Norwegian Sea.

It is clear that offshore hydrophones, even in subpolar regions where the sound channel is not well defined, have lower recording thresholds for small to moderate oceanic events than do onshore seismic stations in the region surrounding an oceanic basin. Therefore, the potential for improving locations of oceanic events, either in water or at the seafloor, is obvious. The actual decrease in location uncertainty depends directly on the number and distribution of offshore receivers that can be included in a location inversion. For the Norwegian Sea study, we detected 2-3 orders of magnitude more events than were located by onshore seismic arrays. We located about 20% of the acoustically detected events to within 10-20km when only T-wave arrivals from a small number of regional receivers were used in the analysis.

Section 6
References

Aki, K. and P.G. Richards, Quantitative seismology: Theory and methods, W.H. Freeman and Co., San Francisco, California, 1980. (UNCLASSIFIED)

Biot, M.A., The interaction of Rayleigh and Stoneley waves in the ocean bottom, Bull. Seismol. Soc. Am., 42, 81-93, 1952. (UNCLASSIFIED)

Blackman, D.K.; Nishimura, C.E.; Orcutt, J.A., Seismoacoustic recordings of a spreading episode on the Mohns Ridge, J. Geop. Res., 105, 10961-73, 2000. (UNCLASSIFIED)

Brekhovskikh, L.M., and Yu. P. Lysanov, Fundamentals of Ocean Acoustics 2nd ed., SpringerVerlag, Berlin, 1982. (UNCLASSIFIED)

Collins, M.D., The adiabatic mode parabolic equation, J. Acoust. Soc. Am., 94, 2269-2278, 1993. (UNCLASSIFIED)

Collins, M.D., McDonald, B.E.; Heaney, K.D.; Kuperman, W.A., Three-dimensional effects in global acoustics, J. Acoust. Soc. Am., 97, 1567-1575, 1995. (UNCLASSIFIED)

de Groot-Hedlin, C.D., and J.A. Orcutt, Synthesis of earthquake-generated T-waves, Geop. Res. Lett., 26, 1227-1230, 1999. (UNCLASSIFIED)

D'Spain, G.L., L.P. Berger, and W.A. Kuperman, Normal mode composition of earthquake Tphases, Pure and Appl. Geop. 158, 475-512, 2001. (UNCLASSIFIED)

Fox, C.G., Dziak, R.P., Matsumoto, H., and A.E. Schreiner, Potential for monitoring low-level seismicity on the Juan de Fuca Ridge using military arrays, Mar. Tech. Soc. J., 27, 22-30, 1994. (UNCLASSIFIED)

Fox, C.G.; Dziak, R.P., Internal deformation of the Gorda Plate observed by hydroacoustic monitoring, J. Geop. Res., 104, 17603-15, 1999. (UNCLASSIFIED)

Hamilton, E.L., Vp/Vs and Poisson's ratio in marine sediments and rocks, J. Acoust. Soc. Am., 66, 1093-1101, 1979. (UNCLASSIFIED)

Hamilton, E.L., Geocoustic modeling of the sea floor, J. Acoust. Soc. Am., 68, 1313-1340, 1980. (UNCLASSIFIED)

Heaney, K, W. Kuperman, and B. McDonald, Perth-Bermuda sound propagation (1960); Adiabatic mode interpretation, J. Acoust. Soc. Am., 90, 2586-2594., 1991. (UNCLASSIFIED)

Herzfeld, U.C., I.I. Kim, and J.A. Orcutt, Is the ocean floor a fractal?, Math. Geol., 27, 421-462, 1995. (UNCLASSIFIED)

Ingenito, F., Measurement of mode attenuation coefficients in shallow water, J. Acoust. Soc. Am., 53, 858-863, 1973. (UNCLASSIFIED)

Jensen, F.B. Kuperman, W.A., Porter, M.B., and Schmidt, H., Computational Ocean Acoustics, American Institute of Physics, Woodbury, New York, 1994. (UNCLASSIFIED)

Johnson,R.H., J. Northrup, and R. Eppley, Sources of Pacific T-Phases, J. Geophys. Res., 68, 42514260, 1963. (UNCLASSIFIED)

Johnson, R.H., Norris, R.A., and Duennebier, F.K., Abyssally generated T-phases, in The Crust and Upper Mantle of the Pacific Area, edited by L. Knopoff, C.L. Drake, and P.J. Hart, Am. Geophys. Union Geophys. Mono. 12, 70-78, 1968. (UNCLASSIFIED)

Johnson, R.H., and R.A. Norris, T-phase radiators in the Western Aleutians, Bull. Seismol. Soc. Am., 58, 1-10, 1968. (UNCLASSIFIED)

Keenan, R.E., and Merriam, L.R.L., Arctic abyssal T phases: Coupling sesimic energy to the ocean sound channel via under-ice scattering, J. Acoust. Soc. Am., 89, 1128-1133, 1991. (UNCLASSIFIED)

Kuperman, W.A., and H. Schmidt, Self-consistent perturbation approach to rough surface scattering in stratified elastic media, J. Acoust. Soc. Am., 86, 1511-1522, 1989. (UNCLASSIFIED)

Levitus and Boyer, World Ocean Atlas 1994, NOAA Atlas NESDIS 4, Washington D.C., 1994. (UNCLASSIFIED)

Mackenzie, Nine term equation for sound speed in the ocean, J. Acoust. Soc. Am., 70, 807, 1993. (UNCLASSIFIED)

McDonald, B.E., M.D. Collins,W.A. Kuperman, and K.D. Heaney, Comparison of data and model predictions for Heard Island acoustic transmission, J. Acoust. Soc. Am., 96, 23572370, 1994. (UNCLASSIFIED)

Milne, A.R., Comparison of spectra of an earthquake T-phase with similar signals from nuclear explosions, Bull. Seismol. Soc. Am., 49, 317-330, 1959. (UNCLASSIFIED)

Munk, W.H., and F. Zachariasen, Refraction of sound by islands and seamounts, J. Atmos. and Oceanic Tech., 8, 554-574, 1991. (UNCLASSIFIED)

Nishimura, C.E. and D.M. Conlon, IUSS dual use: monitoring whales and earthquakes using SOSUS, Mar. Tech. Soc. 27, 13-21, 1994. (UNCLASSIFIED)

Park, M. and R.I. Odom, 1999, The effect of stochastic rough interfaces on coupled-mode elastic waves, Geophys. J. Int., 136, 123-143. (UNCLASSIFIED)

Rayleigh, Lord [J.W. Strutt], The Theory of Sound, Vols. 1 and 2 (2nd Ed., 1894), published in one volume by Dover, New York, 1945. (UNCLASSIFIED)

Schreiner, A.E.; Fox, C.G.; Dziak, R.P., Spectra and magnitudes of T-waves from the 1993 earthquake swarm on the Juan de Fuca Ridge, Geop. Res. Lett., 22, 139-42, 1995. (UNCLASSIFIED)

Shurbet, D.H., and M. Ewing, T-phases at Bermuda and transformation of elastic waves, Bull. Seismol. Soc. Am., 47, 251-262, 1957. (UNCLASSIFIED)

Smith, W.H.F., and Sandwell, D.T., Global sea floor topography from satellite altimetry and ship depth soundings, Science, 277, 1956-1962, 1997. (UNCLASSIFIED)

Spudich, P., and J. Orcutt, Petrology and porosity of an oceanic crustal site: results from wave form modeling of seismic refraction data, J. Geop. Res., 85, 1409-1433, 1980. (UNCLASSIFIED)

Talandier, J., and E.A. Okal, Identification criteria for sources of T-waves recorded in French Polynesia, Pure and Appl. Geop., 158, 567-604, 2001. (UNCLASSIFIED)

Talandier, J. and E.A. Okal, On the mechanism of conversion of seismic waves to and from T waves in the vicinity of Island Shores, Bull. Seismol. Soc. Am., 88, 621-632, 1998. (UNCLASSIFIED)

Vogt, P.R., Geophysical and geochemical signatures and plate tectonics, in The Nordic Seas, B.G. Hurdle (ed.), Springer-Verlag, New York, 413-628, 1986. (UNCLASSIFIED)

Walker, D. A., C. S. McCreery, and Y. Hiyoshi, T-phase spectra, seismic moments, and tsunamigenesis, Bull. Seismol. Soc. Am., 82, 1275-1305, 1992. (UNCLASSIFIED)

DEPARTMENT OF DEFENSE

DEFENSE TECHNICAL INFORMATION CENTER
8725 JOHN J. KINGMAN, RD SUITE 0944
FORT BELVOIR, VA 22060 6218
2 CYS   ATTN: DTIC/OCP

DIRECTOR
DEFENSE INTELLIGENCE AGENCY
BUILDING 6000, BOLLING AFB
WASHINGTON, DC 20340 5100
        ATTN: DTIB

DIRECTOR
DEFENSE RESEARCH & ENGINEERING
WASHINGTON, DC 20301 - 3110
        ATTN: DDR&E, RM 3E808

DEFENSE THREAT REDUCTION AGENCY
44965 AVIATION DRIVE
DULLES, VA 20166 - 7517
        ATTN: TDC, M. SHORE
        ATTN: TDCN, DR. R. GUSTAFSON
        ATTN: TDCN, DR. S. MANGINO
        ATTN: TDCN, DR. ANTON DAINTY

OFFICE OF THE SECRETARY OF DEFENSE
NUCLEAR TREATY PROGRMS OFFICE
1515 WILSON BOULEVARD, SUITE 720
ARLINGTON, VA 22209
        ATTN: DR. R. ALEWINE, III

DEPARTMENT OF THE AIR FORCE

AIR FORCE RESEARCH LABORATORY
5 WRIGHT STREET
HANSCOM AFB, MA 01731 - 3004
        ATTN: RESARCH LIBRARY/TL

AIR FORCE TECHNICAL APPLICATION CENTER
1300 17TH STREET SUITE 1450
ARLINGTON, VA 22209
        ATTN: ROBERT BLANDFORD

AIR FORCE TECHNICAL APPLICATIONS CTR
1030 S. HIGHWAY AIA
PATRICK AFB, FL 32925 3002
        ATTN: CA/STINFO
        ATTN: DEAN CLAUTER, TTER
        ATTN: DR. BOB KEMERAIT
        ATTN: DR. DAVID RUSSELL
        ATTN: GEORGE ROTHE, TTR
        ATTN: MR. MATTHEW SIBOL
        ATTN: VINDELL HSU, TTR

DEPARTMENT OF ENERGY

UNIVERSITY OF CALIFORNIA
LAWRENCE LIVERMORE NATIONAL LAB
P.O. BOX 808
LIVERMORE, CA 94551 9900
        ATTN: DR D. HARRIS, MS L -205
        ATTN: KEITH NAKANISHI
        ATTN: L - 103, W.J. HANNON, JR
        ATTN: TECHNICAL STAFF, MS L - 200
        ATTN: TECHNICAL STAFF, MS L - 208
        ATTN: TECHNICAL STAFF, MS - 205

LOS ALAMOS NATIONAL LABORATORY
P.O. BOX 1663
LOS ALAMOS, NM 87545
        ATTN: FRANCESA CHAVEZ, MS - D460
        ATTN: MS - F 607, D. STEEDMAN
        ATTN: TECHNICAL STAFF, MS C335
        ATTN: TECHNICAL STAFF, MS F665

PACIFIC NORTHWEST NATIONAL LABORATORY
P.O. BOX 999
BATTELLE BOULEVARD
RICHLAND, WA 99352
        ATTN: MS K5-12, DAN N HAGEDORN

SANDIA NATIONAL LABORATORIES
ATTN: MAIL SERVICE
P.O. BOX 5800
ALBUQUERQUE, NM 87185 - 1363
        ATTN: TECHNICAL STAFF, DEPT 9311
            MS 0813
        ATTN: TECHNICAL STAFF, DEPT 5732
            MS 0979
        ATTN: TECHNICAL STAFF, DEPT 5704
            MS 0655
        ATTN: TECHNICAL STAFF, DEPT 5736
            MS 0572

OTHER GOVERNMENT

DEPARTMENT OF STATE
OES/NEP, ROOM 782-8
2201 C STREET, NW
WASHIINGTON, DC 20520
    ATTN: M. DREILER, RM 4953
    ATTN: R. MORROW, RM 5741

US GEOLOGICAL SURVEY
ADVANCED SYSTEMS CENTER
MS 562
RESTON, VA 20192
    ATTN: DR. JOHN FILSON
    ATTN: W. LEITH

DEPARTMENT OF DEFENSE CONTRACTORS

BBN CORPORATION
1300 N 17TH STREET SUITE 1200
ARLINGTON, VA 22209
    ATTN: DR. D. NORRIS
    ATTN: HEODORE FARRELL
    ATTN: JAY PULLI

CENTER FOR MONITORING RESEARCH
1300 N 17TH STREET SUITE 1450
ARLINGTON, VA 22209
    ATTN: DR. K. L. MCLAUGLIN
    ATTN: DR. R. WOODWARAD
    ATTN: DR. ROBERT NORTH
    ATTN: DR. V. RYABOY
    ATTN: DR. X. YANG
    ATTN: LIBRARIAN

ENSCO, INC
4849 N. WICKHAM RD
MELBOURNE, FL 32940
    ATTN: DR. DAVID TAYLOR

ENSCO, INC.
P.O. BOX 1346
SPRINGFIELD, VA 22151 - 0346
    ATTN: DOUGLAS BAUMGARDT
    ATTN: ZOLTAN DER

GEOPHEX, LTD.
WESTON GEOPHYSICAL CORP
57 BEDFORD ST SUITE 102
LEXINGTON, MA 02420
    ATTN: DR. DELAINE REITER
    ATTN: MR. JIM LEWKOWICZ

ITT INDUSTRIES
ITT SYSTEMS CORPORATION
1680 TEXAS STREET SE
KIRTLAND AFB, NM 87117 - 5669
2 CYS   ATTN: DTRIAC
    ATTN: DARE

MAXWELL LABORATORIES, INC.
S-CUBED WASHINGTON RESEARCH OFFICE
11800 SUNRISE VALLEY DRIVE
SUITE 1212
RESTON, VA 22091
    ATTN: DR. THOMAS J. BENNETT

MISSION RESEARCH CORP
8560 CINDERBED ROAD
SUITE 700
NEWINGTON, VA 22122
    ATTN: DR. MARK FISK

MISSION RESEARCH CORP
P.O. DRAWER 719
SANTA BARBARA, CA 93102 - 0719
    ATTN: DR. S. BOTTONE

MULTIMAX, INC
1441 MCCORMICK DRIVE
LANDOVER, MD 20785
    ATTN: DR. WINSTON CHAN

SCIENCE APPLICATIONS INTL CORP
10260 CAMPUS POINT DRIVE
SAN DIEGO, CA 92121 -1578
    ATTN: DR. A. BAKER
    ATTN: DR. G. KENT
    ATTN: DR. J. STEVENS
    ATTN: DR. THOMAS C. BACHE, JR.
    ATTN: DR. THOMAS J. SERENO, JR.

ST LOUIS UNIVERSITY
P O BOX 8148
PIERRE LACLEDE STATION
ST LOUIS, MO 63156 - 8148
    ATTN: PROF. BRIAN J MITCHELL
    ATTN: PROF. BRIAN MITCHELL
    ATTN: PROF. ROBERT HERMAN

TITAN CORPORATION (ATS)
1900 CAMPUS COMMON DRIVE SUITE 600
RESTON, VA 20191 - 1535
    ATTN: DR. CYRUS P. KNOWLES

TEXAS, UNIVERSITY AT AUSTIN
P.O. BOX 7726
AUSTIN, TX 78712
    ATTN: DEPT EARTH PLANET SCI

UNIVERSITY OF CALIFORNIA - SAN DIEGO
SCRIPPS INSTITUTION OF OCEANOGRAPHY
P O BOX 6049
SAN DIEGO, CA 92166 - 6049
    ATTN: CATHERINE DE GROOT-HEDLIN
    ATTN: DONNA BLACKMAN
    ATTN: JOHN ORCUTT

URS CORP CORPORATION
566 EL DORADO STREET
PASADENA, CA 91109 - 3245
    ATTN: DR. BRADLEY B. WOODS
    ATTN: DR. CHANDAN K. SAIKIA

FOREIGN

AUSTRALIAN GEOLOGICAL SURVEY
ORGANIZATION
CORNER OF JERRAGOMRRRA & NINDMARSH
DRIVE
CANBERRA, ACT 2609
AUSTRALIA
    ATTN: DAVID JEPSON

GEOPHYSICAL INSTITUTE OF ISRAEL
POB 182
LOD, 71100 ISRAEL
    ATTN: DR. YEFIM GITTERMAN
    ATTN: DR. A. SHAPIRA

I.R.I.G.M. - B.P. 68
38402 ST. MARTIN D'HERES
CEDEX, FRANCE
    ATTN: DR. MICHEL BOUCHON

MINISTRY OF DEFENSE
PROCURMENT EXECUTIVE
BLACKNESS, BRIMPTON
READING FG7- 4RS ENGLAND
    ATTN: DR. PETER MARSHALL

NTNF/NORSAR
P.O. BOX 51
N-2007 KJELLER, NORWAY
    ATTN: DR. FRODE RINGDAL
    ATTN: TORMOD KVAERNA

OBSERVATORIE DE GRENOBLE
I.R.I.G.M. - B.P. 53
38041 GRENOBLE, FRANCE
    ATTN: DR. MICHEL CAMPILLO

RESEARCH SCHOOL OF EARTH SCIENCES
INSTITUTE OF ADVANCED STUDIES
G.P.O. BOX 4
CANABERRA 2601, AUSTRALIA
    ATTN: PROF BRIAN L.N. KENNETT

RUHR UNIVERSITY/BOCHUM
INSTITUTE FOR GEOPHYSIK
P.O. BOX 102148
463 BOCHUM 1, GERMANY
    ATTN: PROF. HANS - PETER HARJES

UNIVERSITY OF BERGEN
INSTITUTE FOR SOLID EARTH PHYSICS
ALLEGATION 41
N-5007 BERGEN, NORWAY
    ATTN: R. EYSTEIN HUSEBYE

UNIVERSITY OF CAMBRIDGE
DEPT. OF EARTH SCIENCES
MADINGLEY RISE, MADINGLEY ROAD
CAMBRIDGE CB3 OEZ, ENGLAND
    ATTN: PROF. KEITH PRIESTELY

DISTRIBUTION LIST
DTRA-TR-01-33

DIRECTORY OF OTHER (LIBRARIES AND UNIV)

ARIZONA, UNIVERSITY OF
DEPT OF GEOSCIENCES/SASO
TUCSON, AZ 85721
    ATTN: PROF. TERRY C. WALLACE

BOISE STATE UNIVERSITY
GEOSCIENCES DEPARTMENT
1910 UNIVERISTY DRIVE
BOISE, ID 83725
    ATTN:JAMES E ZOLLWEG

BOSTON COLLEGE
INSTITUTE FOR SPACE RESEARCH
140 COMMONWEALTH AVENUE
CHESTNUT HILL, MA 02167
    ATTN: DR. D. HARKRIDER
    ATTN: MR. B. SULLIVAN

BROWN UNIVERSITY
DEPARTMENT OF GEOLOGICAL SCIENCES
75 WATERMAN STREET
PROVIDENCE, RI 02912- 1846
    ATTN: PROF. D. FORSYTH

CALIFORNIA INSTITUTE OF TECHNOLOGY
DIVISION OF GEOLOGY & PLANETARY SCIENCES
PASADENA, CA 91125
    ATTN: PROF. DONALD V. HELMBERGER
    ATTN: PROF. THOMAS AHRENS

UNIVERSITY OF CALIFORNIA BERKELEY
281 MCCONE HALL
BERKELY, CA 94720 2599
    ATTN: PROF. B. ROMANOWICZ
    ATTN:PROF. LANE JOHNSON

UNIVERSITY OF CALIFORNIA DAVIS
DAVIS, CA 95616
    ATTN: R.H. SHUMWAY, DIV
        STATISTICS

UNIVERSITY OF CALIFORNIA SAN DIEGO
LA JOLLA, CA 92093 0225
    ATTN: DR.L. DEGROOT - HEDLIN
    ATTN: DR. M. HEDLIN
    ATTN: PROF. F. VERNON
    ATTN: PROF. J. BERGER
    ATTN: PROF. J. ORCUTT

CALIFORNIA- SANTA CRUZ, UNIVERSITY OF
INSTITUE OF TECTONICS
SANTA CRUZ, CA 95064
    ATTN: DR. RU SHAN WU
    ATTN: PROF. THORNE LAY

COLORADO-BOULDER UNIVERSITY OF
BOULDER, CO 80309
    ATTN MICHAL RITZWOLLER, CAMPUS
        BOX 390
    ATTN: PROF CHARLES ARCHAMBEAU

COLUMBIA UNIVERSITY
LAMONT - DOHERTY EARTH OBSERVATORY
PALISADES, NY 10964
    ATTN: DR. LYNN R. SYKES
    ATTN: DR. JACK XIE
    ATTN: DR. W-Y KIM
    ATTN: PROF. PAUL G. RICHARDS

CONNECTICUT UNIVERSITY OF
DEPT OF GEOLOGY & GEOPHYSICS
STOOR, CT 06269 - 2045
    ATTN: PROF VERNON F CORMIER,
        U-45, RM 207

CORNELL UNIVERSITY
DEPT OF GEOLOGICAL SCIENCES
3126 SNEE HALL
ITHACA, NY 14853
    ATTN: PROF. MUAWIA BARAZANGI

HARVARD UNIVERSITY
HOFFMAN LABORATORY
20 OXFORD STREET
CAMBRIDGE, MA 02138
    ATTN: PROF. ADAM DZIEWONSKI
    ATTN: PROF. GORAN EKSTROM

INDIANA UNIVERSITY
DEPARTMENT OF GEOLOGICAL SCIENCES
1005 10TH STREET
BLOOMINGTON, IN 47405
    ATTN: PROF. G. PAVLIS

IRIS
1200 NEW YORK AVENUE, NW, SUITE 800
WASHINGTON, DC 20005
    ATTN: DR. DAVID SIMPSON
    ATTN: DR. GREGORY E. VAN DER VINK

MASSACHUSETTS INSTITUTE OF TECHNOLOGY
EARTH RESOURCES LABORATORY
42 CARLETON STREET
CAMBRIDGE, MA 02142
    ATTN: DR. W. RODI
    ATTN: PROF. M. NAFI TOKSOZ

MICHIGAN STATE UNIVERSITY LIBRARY
450 ADMINISTRATION BUILDING
EAST LANSING, MI 48824
    ATTN: KAZUYA FUJITA

NEW MEXICO STATE UNIVERSITY
DEPARTMENT OF PHYSICS
LAS CRUCES, NM 88003
    ATTN: PROF. JAMES NI
    ATTN: PROF. THOMAS HEARN

NORTHWESTERN UNIVERSITY
DEPARTMENT OF GEOLOGICAL SCIENCES
1847 SHERIDAN RD
EVANSTON, IL 60208
    ATTN: PROF. E. OKAL

PENNSYLVANIA STATE UNIVERSITY
GEOSCIENCES DEPARTMENT
403 DEIKE BUILDING
UNIVERSITY PARK, PA 16802
    ATTN: PROF. CHARLES A LANGSTON
    ATTN: PROF. SHELTON ALEXANDER

SAN DIEGO STATE UNIVERSITY
DEPARTMENT OF GEOLOGICAL SCIENCES
SAN DIEGO, CA 92182
    ATTN: PROF. STEVEN M. DAY

SOUTHERN METHODIST UNIVERSITY
DEPARATMENT OF GEOLOGICAL SCIENCES
P.O. BOX 750395
DALLAS, TX 75275
    ATTN: B. STUMP, DEPT
    GEOLOGICAL SCIENCES
    ATTN: E. HERRIN, DEPT
    GEOLOGICAL SCIENCES
    ATTN: G MCCARTOR, DEPT
    OF PHYSICS
    ATTN: H L GRAY, DEPT OF
    STATISTICS

UNIVERSITY OF HAWAII
MANOA
P.O. BOX 1599
HAILUA-KONA, HI 96745 - 1599
    ATTN: DR. M. A. GARCES

UNIVERSITY OF IDAHO
DEPARTMENT OF GEOLOGY
MOSCOW, ID 93844
    ATTN: PROF. K. SPRENKE

UNIVERSITY OF SOUTHERN CALIFORNIA
520 SEAVER SCIENCE CENTER
UNIVERSITY PARK
LOS ANGELES, CA 90089 - 0483
    ATTN: PROF C.G. SAMMIS

WASHINGTON UNIVERSITY
ONE BROOKING DRIVE
SAINT LOUIS, MO 63130 - 4899
    ATTN: DR. G. SMITH, DEPT
    EARTH PLANET SCIENCE